Stress Distribution and Fault Development Around Nepal Himalaya by Means of Finite Element Method

Stress Distribution and Fault Development Around Nepal Himalaya by Means of Finite Element Method

Md. Mahmudul Alam and Daigoro Hayashi

Department of Physics and Earth Sciences, University of the Ryukyus, Nishihara, Okinawa, 903-0213, Japan

Abstract

There are a number of methods to analyse geological structures. Finite element method is one of them. Numerical modeling based on finite element analysis is an effective tool for studying the elastic behaviors of earth's crust due to tectonic movement. This study describes how to use an advanced numerical modeling technique, the finite element method, to compute rock deformation and to predict stress and fault development as a function of material properties, cohesion and friction angle. Stress distribution and fault development of 2 dimensional plane strain FEM models of four Himalayan cross sections are described. SW (south west) to NE (north east) horizontal shortening up to maximum 375 m (equivalent displacement at 7.5 cm/yr of 5000 yr) is applied at the southwestern end of the cross-sections. Proposed models show that the direction of maximum principal stresses (σ_1) are horizontal along the shallower part of all the models. Variation of the velocity boundary condition indicates the changes of direction of principal stresses along the deeper part while that along the shallower part remain unchanged.

According to the Mohr - Coulomb criterion, failure is observed along the shallower part of Siwalik, Tethys and Granitic layer, and a very few near the surface of MBT, MCT and STDS. Failure has not occurred in the deeper part of Higher Himalaya and Lesser Himalaya, inspite of changing physical parameters of rock formations, because of the hydrostatic condition that is observed along the models. Previous studies on focal mechanism solutions of earthquakes in the Himalayan region provide the existence of thrust faults along its EW stretching with one plane dipping gently north beneath the Himalaya. Simulation shows the same distribution of thrust faults along the upper part of the models as shown by the focal mechanism solutions.

Abbreviations and Notations

SH : Sub-Himalaya
LH : Lesser Himalaya
LHT : Lesser Himalayan Thrust
LHS : Lesser Himalayan Sequence
HH : Higher Himalayas
HHS : Higher Himalayas Sequence
MBT : Main Boundary Thrust
MBF : Main Boundary Front
MCT : Main Central Thrust

MDT: Main Detachment Thrust
MFT: Main Frontal Thrust
STD : South Tibetan Detachment
STDS: South Tibetan Detachment System
TH : Tethys-Himalayas
TTs : Tibetan Tethys series
IT : Indus Tsangpo
ITS : Indus Tsangpo Suture
Sed. : Sediment
Gn. : Gneiss
NF : Normal fault
FEM: Finite Element Method
σ_1 : Maximum Principal Stress
σ_2 : Intermediate Principal Stress
σ_3 : Minimum Principal Stress

Introduction

The Nepal Himalayas, with an extension of 800 km, cover the mountain ranges lying within the Kingdom of Nepal. Since 1949, when Nepal opened its border to the foreigners, an intense geological investigation has taken place, and in a short time Nepal has become one of the geologically well known tracts of the Himalayan range. The earliest reported visitor was Hooker, who in 1848 crossed the Tamur Vally in eastern Nepal (Hooker, 1854). He was followed by Medlicott, who investigated the Katmandu region and the Trisuli Ganga (Medlicott, 1875). The first comprehensive account of Nepalese geology has been given by Auden (1935). Heim and Gansser (1939) entered northwestern Nepal in 1939. In 1950 Hagen began his field work for the Government of Nepal. During 10 years of intensive investigations in practically all parts of the now accessible kingdom he accumulated a wealth of geological facts, unequal in the history of geological exploration in the Himalayas.

The excellent geological results by Lombard (Swiss Everest expedition) and Bordet's (French ascents of Makalu) expeditions are a valuable contribution of the highest mountain group. In 1962 the Dutch geologists Egeler and De Boy, in early 1963 G. Fuchs of Australian expedition, in late 1963 Bordet with Reymand and Krummenacher covered the Thakkhola region.

Himalayas is the world's highest mountain chain, it constitutes the greatest attraction to climbers and trekkers throughout the world. But more than anything else, the Himalayas represent the awe-inspiring power, beauty, and grandeur of nature. Forming a distinct geographical divide that separates the Indian subcontinent from Central Asia, the Himalayas extend from west to east in a massive arc (Fig. 1) for about 2500 kilometers terminating at the Yunnan and the Pamir syntaxes. Covering an astounding area of 612,021 sq. km,

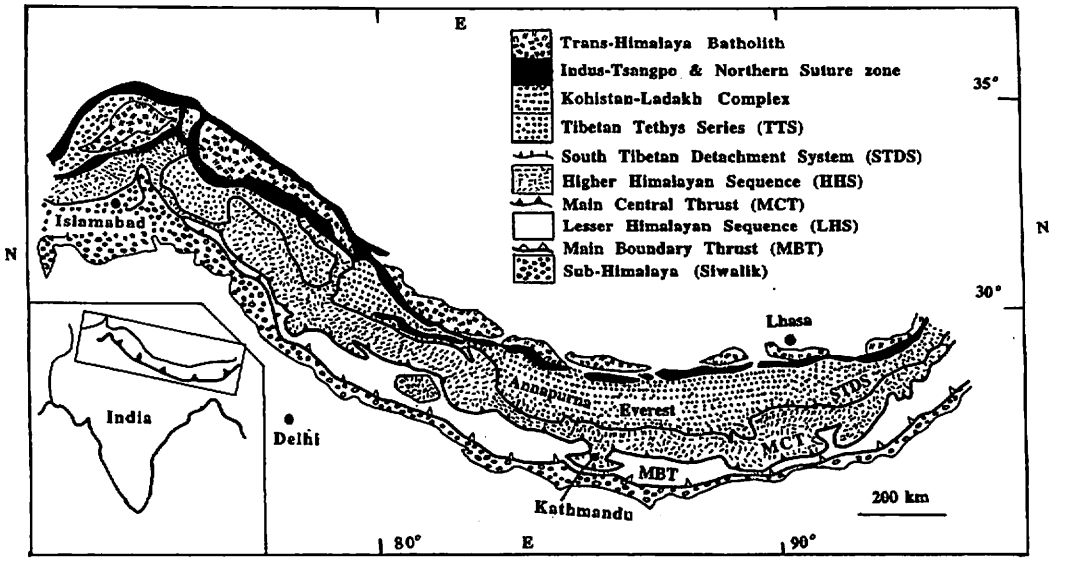

Fig. 1. Simplified geologic map of the Himalaya showing the major tectonostratigraphic divisions. Modified from Gansser (1964), Le Fort (1975), Barnicot and Treloar, Parrish and Hodges, Kaneko (1997).

the vast mountain chain passes through the Indian States of Jammu and Kashmir, Himachal Pradesh, Uttar Pradesh, Sikkim and the Himalayan kingdoms of Nepal and Bhutan. The Tibetan Plateau - the roof of the world - forms the northern boundary of this magnificent mountain system while lower extensions of the Himalayas branch off from eastern and western frontiers of these mountains.

The continent - continent collision model for the uplift of the Tibetan Plateau has been treated numerically by England and others (Engaland and McKenzie, 1982, 1983; England and Houseman 1985, 1986). In this studies, they assumed the Indian and Asian crusts to be incompressible non-Newtonian fluids and analysed the collision in 3-dimension by means of a thin viscous sheet analysis and had the intention of explaining the structure of the interior of the Asian continent. It is impossible, however, to understand the uplift of the Himalayas directly from their model, although it may represents one of the most reasonable collision models.

The largest negative gravity anomalies over the Ganga Basin and the Himalaya are reproduced by a model where the Indian crust underthrusts Himalaya at shallow angles of $15° \pm 5°$ along various thrust zones (Indus Suture Zone, MCT and MBT). In this model the Himalaya region is isostatically uncompensated and the crustal shortening of 300 to 400 km is calculated to have occurred across the mountain (Warsi & Molnar, 1977).

Hayashi (1987, 1988, 1992) numerically simulated the uplift of the Tibetan plateau and the Himalayas assuming that the northerly migration of the Indian plate deforms the overlying Asian continental crust which behaves as an incompressible Newtonian fluid of Asia above the rigid upper mantle. In these models, the upper mantle lithosphere is

a rigid body for the first approximation and the deformable crust overlies the upper mantle. The deformation of the crust is then expected to form plateaus and mountain ranges. Under such an assumption, isostatic readjustment becomes impossible and the calculated values of surface uplift tend to be overestimated. Further, the rigid plate assumption prohibits simulation for a period longer than 0.1 Ma. The numerical technique used in simulation purpose is based on the well known finite element method.

The Himalayas, the world's youngest and highest mountain range, are morphogenetically still active today and up-going. There are basically two causes for this: (i) active faulting in the Siwalik hills in the southern frontal part and (ii) long-wavelength chronic upheaval in the central Higher Himalaya. The uplift of the Siwalik hills is quite a recent event resulting from intermittent earthquakes since the late Pleistocene, whereas the Higher Himalaya started to uplift in association with the MCT active from the middle Miocene and continues to do so at present with episodic rapid rises during the span.

The rise of the mountains shifted successively from the Tibetan Marginal Mountains in the north in the Oligocene to the Higher Himalaya in the Miocene, the Mahabharat Range in the early Pleistocene in association with the southward jump of the thrust faults (*ITS→MCT→MBT→MFT*).

Numerical modeling based on finite element analysis is an effective tool for studying the elastic behaviors of earth's crust due to tectonic (epirogenic and organic) movement. Generally, the deformation that occurs within the earth's crust is inhomogeneous finite deformation. The geological deformation is however too complex to be analyzed.

The strain markers within the rocks and their strain analysis generally provides valuable messages about the nature of tectonic movement which the rock experienced in the past.

Himalaya in Nepal is a complex field where rock sequence are folded, faulted and thrusted in response to a series of upliftment of the Himalaya due to subduction of Indian plate beneath the Eurasia plate. The sedimentary and metamorphic rocks are folded, faulted, jointed and thrusted differently according to the intensity of stress developed within it. The study of these rock sequences and structures certainly may provides various clues to analyse the stress, elastic behavior of the rocks and tectonic history of the region. The aim of the study is to analyse the followings:

(i) The intensity and direction of principal stresses along the Nepal Himalaya are computed in various boundary conditions.

(ii) Development of faults

(iii) Comparison the simulated stress distribution with the focal mechanism solution happened within the region.

1. Geological Setting

The great Himalayas extend for about 2500 km from the Punjab Himalaya in the west to the Arnachal Himalaya in the east along the WNW direction like a bordering wall along the southern edge of the Tibetan Plateau.

The geomorphic cross section in the N-S direction is almost similar throughout the Himalayas. A typical section from the Nepal Himalaya is shown in Fig. 2. From north

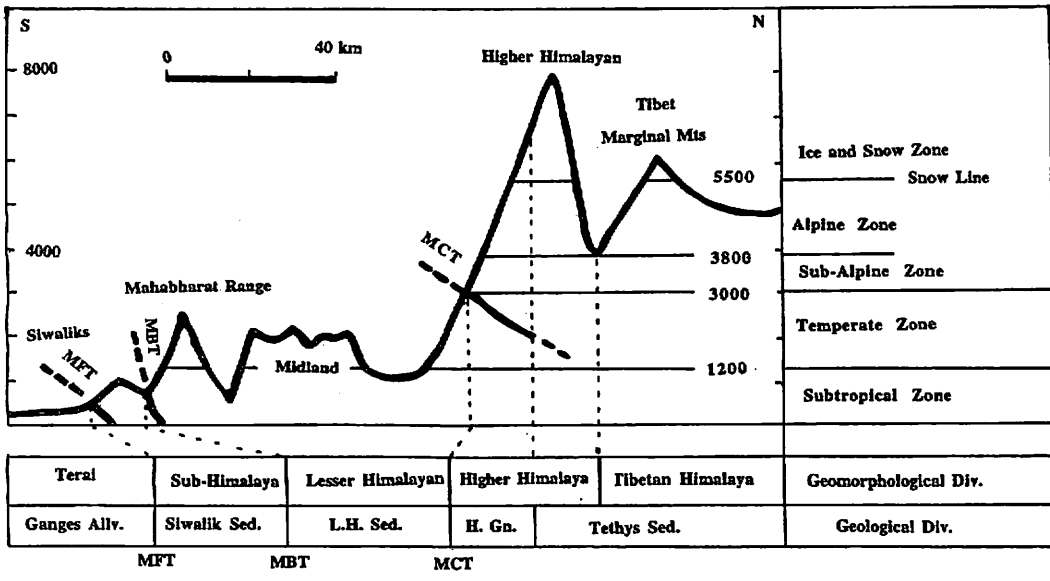

Fig. 2. Simplified cross section of the Himalayas. MFT: Main Frontal Thrust, MBT: Main Boundary Thrust, MCT: Main Central Thrust.

to south, the Tibetan Himalaya (5000 m), the Higher Himalaya (7000-8000 m), the Lesser Himalaya (1500-2000 m) with the Mahabharat Range (3000 m) at the southern border, the Siwalik hills in the Sub-Himalaya (1000 m) and the Terai Plain are zonally arranged.

The geomorphic divisions are well correlated with the zonal distribution of the geologic formations and structural arrangements along the Himalayan trend.

In the Tibetan Himalaya zone in the north, the Tethys sediments of the Palaeozoic to the early Cenozoic age spread over the area which is underlain by a vast amount of granite bodies. The Higher Himalayan zone is occupied by the high mountains covered with snow and glaciers including peaks higher than 8000 m such as Kanchanjangha, Makalu, Everest, Cho-Oyu, Manaslu, Annapurna and Dhaulagiri. The upper parts of these mountains are formed by the Tethys sediments which are underlain by the Central Crystallines composed of high grade metamorphics. Both the sediments and gneisses thrust up the Lesser Himalayan sediments along the MCT (Main Central Thrust), which appears to be one of the significant tectonic boundaries throughout the Himalayas. The lesser Himalayan zone in the Midland is a dissected highland bordered by the Mahabharat Range to the south, made up of the Lesser Himalayan sediments and the Gondwana

sediments as well. The lesser Himalayan sediments of the Precambrian to the early Palaeozoic age show monotonous depositions and are barren in fossils except for a few occurrences of stromatolites. The Sub-Himalayan zone is limited by the MBT (Main Boundary Thrust) to the north along the southern foot of the Mahabharat Range, and the MFT (Main Frontal Thrust) to the south at the southern edge of the Siwalik Group. The Lesser Himalayan sediments thrust up the Siwalik Group of the Sub-Himalaya. The sediments of the Group represent molasse deposits resulted from the rapid upheaval of the Higher Himalaya from the late Tertiary to the early Quaternary. The group has also thrust over the alluvial formation of the Gangetic sediments along the MFT which is presently active along the MBT.

1.1 Evolution of Himalaya

Over two hundred fifty million years ago, India, Africa, Australia, and South America were all one continent called Pangea. Over the next several million years, this giant southern continent proceeded to break up, forming the continents we know today. Pangea essentially turned inside out, the edges of the old continent becoming the collision zones of new continents. Africa, South America, and Antarctica began to fragment.

About 60 million years ago, was the rapid movement of India northward toward the continent of Eurasia. India charged across the equator at rates of up to 15 cm/yr., in the process closing an ocean named Tethys that had separated fragments of Pangea. This ocean is entirely gone today, although the sedimentary rocks that settled on its ocean floor and the volcanoes that fringed its edges remain to tell the tale of its existence.

The Indian subcontinent is moving toward the rest of Eurasian continent at a rate of about 50 mm/yr. (Le Pichon, 1968, Minster et al., 1974). The relative motion of these two continental masses during the past 40 m.y. apparently has caused deformation throughout much of central and eastern Asia, and the creation of the Himalaya are only one consequence of this convergence (Molnar and Tapponnier, 1975). In the early tertiary and ocean basin lay between India and the rest of Eurasia and was part of the Indian plate. Subduction of the Indian plate occurred along the southern margin of the Eurasian continent, until approximately 40 to 50 m.y. ago, when the two continental masses collided with each other (Dewey and Bird, 1970, Le Fort, 1975, Powell and Conaghan, 1973). The low density of crustal rocks together with the much greater thickness of continental than oceanic crust presumably renders simple subduction of continental crust impossible (Isacks et al., 1968, McKenzie, 1969). As a result the convergence of the two continental masses must occur by processes other than subduction - such as crustal shortening and mountain building as in the Himalaya or by lateral movements of large blocks along strike slip faults and out of the way of the impinging continents as in much of the region north of the Himalaya (Molnar and Tapponnier, 1975, Tapponnier and Molnar, 1977).

For at least 80 million years the oceanic Indian Plate continued its inexorable collision

with southern Asia, including Tibet. The heavy ocean floor north of India acted like a giant anchor, plunging rapidly into the mantle, and dragging the Indian continent along with it, northward, towards Tibet.

As the plates collided, the sinking ocean floor generated volcanoes in southern Tibet because the rock at the top of the descending plate melted, from friction and the huge pressures of collision. However, by 25 million years ago the fast moving Indian continent had almost entirely closed over the intervening ocean, squeezing the sediments on the ocean floor. Since the sediments were lightweight, instead of sinking along with the plate, they crumpled into mountain ranges -- the Himalayas.

By 10 million years ago the two continents were in direct collision and the Indian continent, because of its enormous quantity of light quartz-rich rocks, was unable to descend along with the rest of the Indian plate. It was at about this time that the anchor chain must have broken; the descending Indian plate may have fallen off and foundered deep into the mantle. Although we don't fully understand the mechanism of what happened next, it's clear that the Indian continent began to be driven horizontally beneath Tibet like a giant wedge, forcing Tibet upwards. Tibet, meanwhile, is behaving like a giant roadblock that prevents the Himalaya from moving northward.

The Himalayan organic belt has long been regarded as the world standard of an organic belt formed by the collision of two large continents (Dewey and Bird, 1970, Windley, 1984, 1995). For this reason, the Himalayan organic belt has been investigated by many earth scientists, including geologists (Gansser, 1964, Hashimoto et al., 1972, Le Fort, 1975, Stocklin, 1980, Sakai, 1983, 1985, Colchen et al., 1986, Searle et al., 1987, Burchfiel et al., 1992). After the collision between the Indian and Eurasian continents during the Eocene, the large crustal shortening caused by convergence was taken up in major intercontinental subduction which lead to the formation of the Himalayan chain (Pecher, 1989). A series of schematic diagrams in Fig. 3 showing the tectonic evolution of the Himalayan Metamorphic belt in Nepal.

Based on field and laboratory studies, numerical modeling of various aspects of continental collision and ensuing subduction has been achieved (England and Thompson, 1984, Molnar and Tapponier, 1975, Chemenda et al., 1995). Nevertheless, the organic process of the Himalaya mountain range are not yet fully understood.

Future of the Himalaya

Over periods of 5-10 million years, the plates will continue to move at the same rate, which allows us to forecast fairly reliably how the Himalaya will develop. In 10 million years India will plow into Tibet a further 180 km. This is about the width of Nepal. Because Nepal's boundaries are marks on the Himalayan peaks and on the plains of India whose convergence we are measuring, Nepal will technically cease to exist. But the mountain range we know as the Himalaya will not go away. This is because the

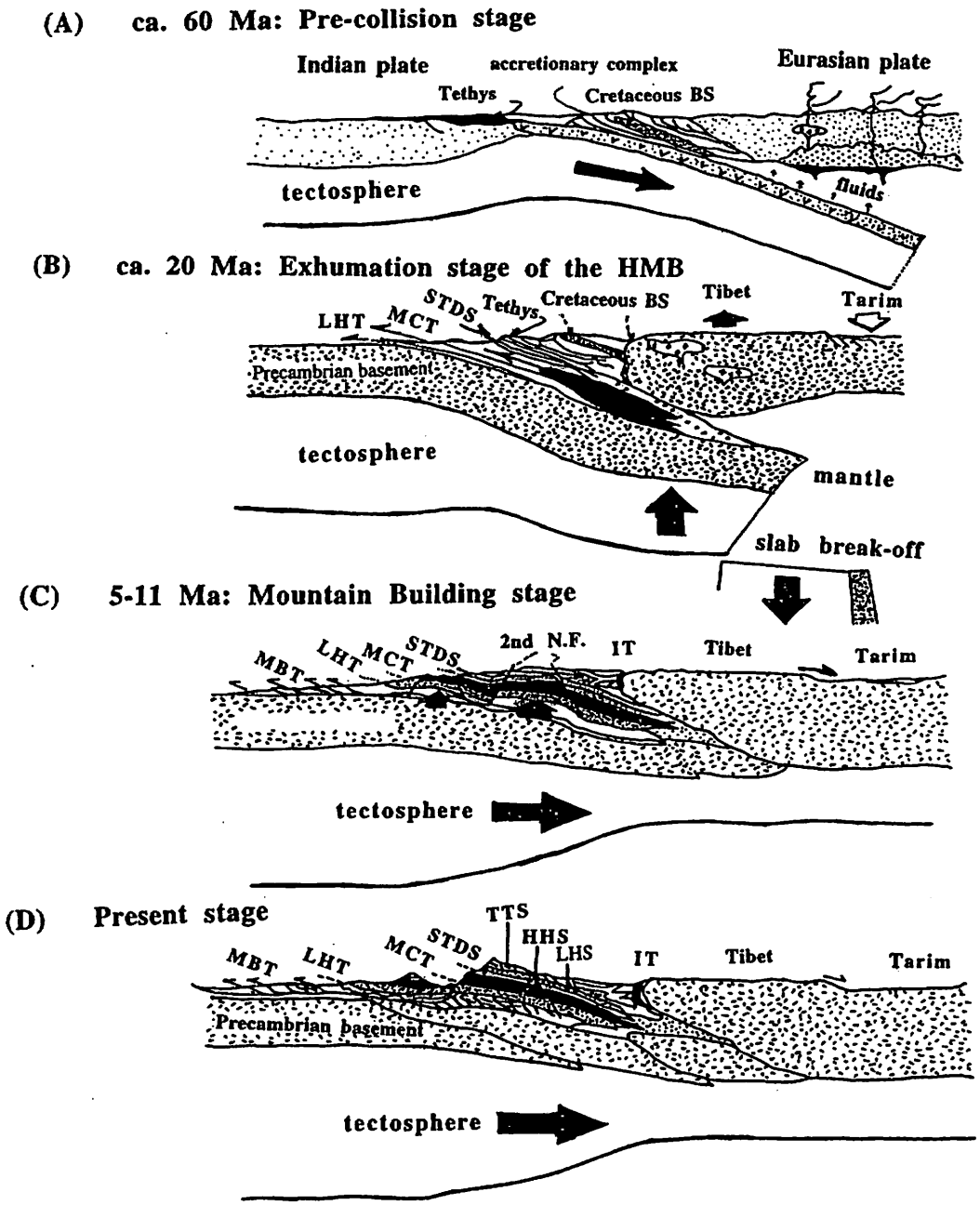

Fig. 3. Schematic diagrams showing the tectonic evolution of the Himalayan Metamorphic belt in Nepal. (A) sub-duction of the Indian continent; (B) subhorizontal extrusion of the HHS and the LHS metamorphic units by synchronous paired normal faulting on the top and reverse faulting (MCT) at the bottom. Tectonic juxtaposition of these metamorphic units at mid-crustal level. (C) & (D) doming of all these three units, by jacking-up due to underthrusting of the sub-Himalayas, and related secondary high-angle normal faulting. Modified from Kaneko (1997).

Himalaya will probably look much the same in profile then as it does now. There will be tall mountains in the north, smaller ones in the south, and the north/south width of the Himalaya will be the same. What will happen is that the Himalaya will have advanced across the Indian plate and the Tibetan plateau will have grown by accretion. One of the few clues about the rate of collision between India and Tibet before the GPS measurements were made was the rate of advance of Himalayan sediments across the Ganges plain. There is an orderly progression of sediments in front of the foothills. Larger boulders appear first, followed by pebbles, and further south, sand-grains, silts, and finally very fine muds. This is what you see when you drive from the last hills of the Himalaya southward 100 km. The present is obvious, but the historical record cannot be seen on the surface because the sediments bury all former traces of earlier sediments. However, in drill holes in the Ganges plain, the coarser rocks are always on the top and the finer pebbles and muds are on the bottom, showing that the Himalaya are relentlessly advancing on India.

1.2 Zonation of the Himalayas

For a proper study, it is necessary to classify the vast area covered by the mountains into smaller sub-sections. The geometric cross section in the N-S direction is almost similar throughout the Himalayas.

The Himalayas can be classified in a variety of ways. From south to north, the mountains can be grouped into four parallel, longitudinal mountain belts (Gansser, 1964), each with its unique features and distinctive geological history:

(i) The Sub Himalayas
(ii) The Lesser Himalayas
(iii) The Higher Himalayas
(iv) The Tethys Himalayas

1.2.1 The Sub-Himalayas

Forming the southernmost belt of the Himalayan range, the Siwaliks are also the lowest and narrowest range in the entire Himalayan system, having an average elevation of about 900 - 1200 m and in places, a width of only 16 km. The Siwaliks rise steeply from the great northern plains of India and Pakistan and run parallel to the main ranges of the Himalayas towards the north, from which they are separated by high mountains and deep valleys. The Sub-Himalayan zone is limited by the Main Boundary Thrust (MBT) to the north along the southern foot of the Mahabharat Range and the Main Frontal Thrust (MFT) to the south at the southern edge of the Siwalik (Churia) Group. The Lesser Himalayan sediments thrust up the Siwalik Group of the Sub-Himalaya. The sediments of the Group represent molasse deposits resulted from the rapid upheaval of the Higher Himalaya from the late Tertiary to early Quaternary. The Group has also

thrust over the alluvial formation of the Gangetic sediments along the MFT which is presently active along with the MBT.

1.2.2 The Lesser Himalayas

The Lesser Himalayas has been variously named the Main central thrust (MCT) zone and Midland sedimentary zone (Arita, 1983), Midland Formation (Le Ford, 1975), Lesser Himalaya (Brunel, 1986) and Lesser Himalayan Sequence (Kaneko, 1994, 1995). Lying between the Higher Himalayas region in the north and the Siwaliks to the south, the Lesser Himalaya region forms the middle section of the Himalayan mountain chain. Lower than the Higher Himalayas or the Great Himalayas, this region has an average altitude of 3700 - 4500 m above sea level. It extends southeast from Pakistan and extends through large parts of the Indian states of Jammu and Kashmir, Himachal Pradesh, Western Uttar Pradesh, Nepal and the North-Eastern Himalayas. The Lesser Himalayan zone in the Midland is a dissected highland bordered by the Mahabharat range to the south, made up of the Lesser Himalayan sediments and the Gondwana sediments as well. The Lesser Himalayan sediments of the Precambrain to the Early Palaeozoic age show monotonous depositions and are barren in fossils except for a few occurrences of stromatolites, while the Gondwana sediments of the Palaeozoic to the Early Tertiary age have abundant fossils which are scattered and exhibit a narrow distribution along faults in some places.

The upper part of the Lesser Himalayan Sequence rocks are mylonitic with localized foliation-parallel bands of high strain. The rock types including psammitic schist, augen gneiss, phyllite, pelitic schist, calc-silicate schist, marbel, siliceous schist and amphibolite.

1.2.3 The Higher Himalayas

The Higher Himalayas is bounded to the south by the Main central thrust (which separates it from the Lesser Himalayan sequence) and to the north by the South Tibetan detachment system. The South Tibetan detachment system, a series of normal faults on the northern flank of the Himalaya, forms the contact between the Tibetan Tetyes sediment and underlying Higher Himalayan Sequence (Burchfiel et al., 1992, BurgChen, 1984, Richard and Jeffrey, 1993, Hashimoto et al., 1973). The Higher Himalaya has been variously named Himalayan Gneiss zone (Arita, 1983), Tibetan slab (Le Ford, 1975, Bordet et al., 1971), and Higher Himalayan Sequence (Kaneko, 1994, 1995), Upper Crystalline Nappe (Fuchs & Frank, 1970), Kathmandu Nappes and Khunbu Nappes (Hagen 1969). The northernmost, longest and the most continuous belt in the Himalayan system, the Higher Himalayan belt forms the backbone of the Himalayas. Lying well above the snow line with an average elevation of about 6100 m (20,000 ft), the Higher Himalaya dominates the extreme northern frontiers of India and the entire northern boundary of Nepal. It rises to its maximum height in Nepal containing nine of the fourteen highest peaks in

the world, all above 8000 m above sea level. The upper parts of these mountains are formed by the Tethys sediments which are underlain by the Central Crystalline composed of high grade metamorphic rock. Both the sediments and gneisses thrust up the Lesser Himalayan sediments along the Main Central Thrust (MCT), which appears to be one of the significant tectonic boundaries throughout the Himalayas. Both groups have slipped and spread over the MCT to the south producing nappe and klippe on the Lesser Himalayan sediments in the Midland.

1.2.4 The Tethys Himalayas

In the Tibetan Himalayan zone, the Tethys sediments of the Palaeozoic to the early Cenozoic age are distributed along the southern most margin of the huge Tibetan Tethys basin, such as the Sagarmatha region, the Langu-Manang basin, the Saipal - Amlang basin, the Spiti basin and the Kashimir basin which is underlain by a vast amount of granite bodies. The northern border of the Tethys sediments is represented by a fault zone which stretches along the Indus and Tsangpo rivers; referred to as the Indus-Tsangpo Suture, which signifies the collision trace of the Indian subcontinent with Eurasia. Some time ago, the Gondwana sediments attributed to the Indian subcontinent were reported from the area lying to the north of the suture zone. It is possible that another collision trace of the continents older than the Indus-Tsangpo Suture exists.

1.3 Lithostratigraphy of Nepal Himalaya

According to the geologist and geophysicists those who surveyed and till now engaged in different parts of Nepal Himalaya, such as Arita, Hayashi and Yoshida (1982), Sako et al. (1968), Hashimoto et al. (1973), Hagen (1969), Fuchs & Frank (1970), Gansser (1964), Bordet et al. (1971), surveyed the Pokhara-Piuthan area, Central Nepal; Kano (1977, 1980 & 1982), Pecher and Le Fort (1977), surveyed the main central thrust zone of the Annapurna Range, Central Nepal; Arita & Yoshida (1982), Sako et al. (1968), Hashimoto et al. (1973), Hagen (1969), Fuchs & Frank (1970), surveyed the Ramdighat, Central Nepal; Yoshida & Arita (1982), Wadia (1975), Tandon (1976), Tandon and Narayan (1981), Opdyke et al. (1979), Johnson et al. (1979), Gill(1952), Gansser (1964), Powel & Conaghan (1973), Siwalik range, Central Nepal; Iwata, Yamanaka & Yoshida (1982), Hazen (1968), Bordet et al. (1971), Le Fort (1976), Takkhola region, Central Himalaya; Yamanaka & Iwata (1982), Hiroshima (1976), Sharma et al. (1980), Hagen (1969), Le Fort (1976), Middle Kali Gandaki and Marsyandi khola, Central Nepal; Yamanaka, Yoshida & Arita (1982), Horman (1974), Hagen (1969), Pokhara Vally, Central Nepal; Yokoyama & Omura (1982), Dana and Kerabari, Central Nepal; Kamada, Arita & Yoshida (1982), Reed (1908), Arkell (1965), Hagen (1968), Bordet et al. (1971), Gansser (1964) and Ryf (1962), Muktinath region, Central Nepal; the lithostatigraphy of the Nepal Himalaya can be summarized in the following table-

Table 1. Geological units and age of rocks in Nepal Himalaya (Gansser, 1964, 1983, Valdia, 1980, Sinhi and Roy, 1982).

Himalaya	Zone	Group	Geological age of rocks
Sub Himalaya	Main Boundary Thrust	Siwalik	Tertiary to Quarternary molasse sediments
Lesser Himalaya	Main Central Thrust	Midland	Mainly Eocambrian clastic sediments with limestone and quartzite, mostly altered to phyllite and metasandstone
Higher Himalaya	Unconformity	Himalayan Gneiss	Rejuvenated Precambrian basement, mostly polymetamorphosed and migmatized at the Alpine stage by the intrusion of tourmaline granites
Tibetan Himalaya	Indus-Tsangpo Suture	Tibetan Tethys	Mainly lower Paleozoic to Mesozoic clastic and calcareous sediments

1.3.1 Siwalik (Churia) Group

The Churia group can be divided on the basis of lithologic nature into three parts, i.e., the lower, the middle and the upper formations. Three divisions of the Churia group were also attempted by Itihara et al. (1972), Hagen (1969), Wadia (1975), West et al., (1978 & 1981), Glennie and Ziegler (1964) divided the Siwaliks in Nepal into the lower "sandstone Facies" and the upper "Conglomerate Facies".

The lower formation consists of irregularly alternating beds of muddy, fine sandstone and siltstone. Variegated siltstones and coaly, black siltstones are intercalated frequently. Sandstone is moderately indurated.

The middle formation consists mainly of thick bedded massive sandstone and subordinately of siltstone and thin-bedded alternation of sandstone and siltstone. Variegated siltstone, irregular-bedded, are sometimes intercalated. Sandstone is less indurated, medium to sometimes coarse-grained white rock with black specks (mostly of biotite), showing a salt-and-pepper appearance. There are also found well-consolidated calcareous sandstone beds which exhibit some concretionary structures. Sandstone is abundant in mica, rare in clay matrix and partly calcite-cemented, belonging to lithic arenite.

The upper formation is composed predominantly of gravel beds and subordinately of sand and silt layers. Mostly they are unconsolidated. Well consolidated calcareous sandstone beds are rarely found in the upper part. Gravels range in size from pebble to boulder and cobble gravels are common. According to Arita et al. (1984, Arjun Khola, Jajarkot-Piuthan area) the lower part of the Churia Group consists mainly of "brick colored" fine- to medium-grained sandstone and contains some intercalations of muscovite-bearing coarsed-grained sandstone. The middle part is made up of the fine- to medium-grained calcareous sandstone in the lower portion and to fine- to medium-grained brick colored mottled sandstone in the upper portion. The upper part is largely composed of conglomerate.

Sub-angular to sub-round and pebble- to cobble-size gravels consists of brick, grey and white cherty quartzite consists of grey limestone and calcareous sandstone and black shaly slate.

In the Karnali-Bheri region, sandstone, mudstone, conglomirate and limestone are found (Hayashi, Fujii, Yoneshiro, & Kizaki, 1984, Valdiya, 1977-78, 1982, Fuchs & Frank, 1970, Fuchs, 1977, 80, and Bashya, 1981).

1.3.2 Midland group

The group is roughly divided into two sub-groups; the quartzite and sandstone subgroup and the sandstone and phyllite subgroup (Kawamitsu & Hayashi, 1991, Annapurna region).

The quartzite and sandstone subgroup is mainly composed of quartzite with sandstone interbeds. The quartzite is white in color, including muscovite, biotite and plagioclase. Crenulation cleavages are shown on bedding planes.

The sandstone and phyllite subgroup is mainly exposed in the Midland area. The group consists mainly of biotite bearing black phyllite with quartz veins. Crenulation cleavages and kink folds are seen on bedding planes.

According to Arita et al. (1984, Jajarkot-Piuthan area), Sakai (1982-84, Tansen area), Gansser, 1964, Hagen, 1969, Hashimoto et al., 1973 and Fuchs & Frank, 1970 (Jajarkot area), Garnet-mica-chlorite phyllite schist, black-green phyllite, crystalline limestone, blastomylonitic augen gneiss, limestone, dolomite, calcareous sandstone are found in the Jajarkot Crystalline klippe. Quartz, sandstone, green phyllite, black phyllite, slate, shale, dolomite, limestone and calcareous shale, conglomerate and amphibolite are found in the Dunaihi, Maikot and Roli-Sallyan area. And Quartz, sandstone, shale, dolomite, limestone and variegated rocks are found in the Piuthan, Musikot, Dalli and Dhorpatan zone. Blastomylonitic augen gneisses also observed on the Bheri river just south of Jajarkot (Hayashi et al., 1984).

Phyllite, quartzite/quartz-conglomerate, siliceous sandstone, amphibolite, limestone and slate are found in the Karnali-Bheri region (Hayashi, Fujii, Yoneshiro, and Kizaki, 1984, Valdiya, 1977-78, 1982, Fuchs and Frank, 1970, Fuchs, 1977, 80, and Bashya, 1981).

1.3.3 Main Central Thrust Group (MCT Group)

The group has inserted and consists of the black and green phyllite subgroup, augen gneiss I subgroup, amphibolite subgroup, quartzite subgroup and calcarious phyllite schist subgroup (Kawamitsu & Hayashi, 1991, Annapurna region).

The black and green phyllite subgroup is commonly exposed in the area and is composed of biotite-graphite-phyllite, wavy green phyllite and biotite-chlorite phyllitic schist with or without garnet. The phyllitic schist is characterized by wavy micaceous layers with irregular folded lenticular quartz aggregates. The typical mineral assemblage is

garnet-biotite-muscovite-K feldspar-plagioclase-quartz.

The augen gneiss I subgroup is seen at Ulleri along the Kali Gondaki river. The augen gneiss consists of medium to coarse-grained minerals. The augen structure comprises K feldspar-porphyroblasts and/or porphyroclasts. The gneiss was called Ulleri augen gneiss by Le Fort. The representative mineral assemblage is biotite-muscovite-K-feldspar-plagioclase-quartz. The amphibolite subgroup; several amphibolite sheets are placed between the lower and middle parts of the MCT group. Typical mineral assemblage is hornblend-biotite-quartz-K feldspar.

The quartzite subgroup; a few quartzite layers are placed between the middle horizons of the MCT group along the Kali Gandaki and Modi Khola rivers. The colors of the quartzites are white, bluish grey and green. These quartzite are fine to medium-grained sand size, including thin micaceous layers. The calcareous phyllite-schist subgroup is exposed close to the upper MCT.

Limestone, garnet two mica-schist/quartzite, granite are found in the Karnali-Bheri region (Hayashi, Fujii, Yoneshiro, and Kizaki, 1984, Valdiya, 1977-78, 1982, Fuchs and Frank, 1970, Fuchs, 1977, 80, and Bashya, 1981).

1.3.4 Himalayan Gneiss Group

The group consists of various kinds of gneisses and thrusts over the MCT group along the upper MCT. The group is based on the field survey, divided into three subgroups; gneiss I, gneiss II and augen gneiss II subgroups (Kawamitsu & Hayashi, 1991, Annapurna region). Structure of these gneisses is generally concordant with that of the upper MCT.

The gneiss I subgroup; basal part of the Himalayan Gneiss group is composed of the gneiss I subgroup, which is represented by the alternation of pelitic and psammitic gneisses. The pelitic gneiss possesses medium to coarse-grained minerals, especially garnet, while the psammitic gneiss consists of fine-grained particles. The typical mineral assemblage is garnet-biotite-muscovite-K feldspar-plagioclase-quartz.

The gneiss II subgroup is composed of fine to medium grained calc-silicate gneiss and overlies the gneiss I subgroup. The typical mineral assemblage is biotite-muscovite-kyanite-calcite-plagioclase-quartz.

The augen gneiss II subgroup which is composed of migmatic gneiss with augen structure, occupies the upper part of the Himalayan Gneiss group. The typical mineral assemblage is biotite-muscovite-K feldspar-quartz.

According to Sakai (1982-84, Tansen area), Gansser, 1964, Hagen, 1969, Hashimoto et al., 1973 and Fuchs & Frank (1970, Jajarkot area), the basal part of the gneisses consists of mylonitize gneiss including crushed garnet porphyroblasts and is followed by the kyanite-garnet-mica gneiss. The "argillo-arenaceous" gneiss gradually grade upward into calcareous gneisses of the middle calcareous gneisses in the northeast. According to Arita et al.

(1984, Jajarkot Dailekh -Rara area), the Himalayan gneisses are made up of garnet-mica gneiss, kyanite-garnet-mica gneiss, siliceous gneiss and calcareous gneiss.

Migmatite gneiss, Augen gneiss, calc-siliceous gneiss, garnet biotite gneiss are found in the Karnali-Bheri region (Hayashi, Fujii, Yoneshiro, and Kizaki, 1984, Valdiya, 1977-78, 1982, Fuchs & Frank, 1970, Fuchs, 1977, 80, and Bashya, 1981).

1.3.5 Tibetan Tethys Group

The group is composed of the crystalline limestone subgroup and the alternation of quartzite and mudstone subgroup (Kawamitsu & Hayashi, 1991, Annapurna region). The group overlies the Himalayan Gneiss group and seems to be intensely deformed. The group is called the Larjung Formation by Bordet et al. (1980).

The crystalline limestone subgroup; basal part of the Tibetan Tethys group is represented by the non fossiliferous crystalline limestone subgroup. The alternation of quartzite and mudstone subgroup overlies the crystalline limestone subgroup.

The sedimentary rocks of the Tibetan Tethys basin extend from the highest part of the great Himalayas to the north in the Chinese Tibetan territory, overlying the Himalayan gneisses which are thrusted southwards onto the Midland metasediments. The rocks of this basin discussed separately from the Midland meta-sedimentary basin and tectonic units independent from those of the Midland (Hagen, 1969 and Fuchs, 1967). Rocks found in the Kali Gandaki, Shisha Pangma, Sagarmatha and Dhaulagiri area are impure limestone, dolomite, argillaceous and calcareous pelitcs.

The calcareous schist is found in the Karnali-Bheri region (Hayashi, Fujii, Yoneshiro, and Kizaki, 1984, Valdiya, 1977-78, 1982, Fuchs & Frank, 1970, Fuchs, 1977, 1980, and Bashya, 1981).

2. Numerical Simulation

2.1 Finite Element Method (FEM)

Finite element method is a well known method broadly using in most of the branches of applied sciences, Engineering, Medical sciences or even in Economics. It is also rapidly using for numerical calculation in structural geology and tectonics.

An adequate model is obtained using a finite number of well defined components in many situations and such problem is known as discrete. In other words, the subdivision is continued indefinitely and this leads to differential equations or equivalent statements which imply an infinite number of elements and such system is termed as continuous.

As the capacity of all the computers is finite, discrete problem can be solved readily (even if the sample size is large) but continuous problem can only be solved exactly by mathematical manipulation. The first have developed general techniques applied directly to differential equations governing the problem such as finite difference approximation (R.V. Southwell, 1946, D.N.DE.G. Allen, 1955), various weighted residual procedures

(S.H. Crandall, 1956, B.A. Finlayson, 1972). In the field of solid mechanics, reasonably good solution to a continuum problem can be obtained by substituting small portions (elements) of the continuum by an arrangement of simple elastic bars (McHenry, 1943, Itrenikoff, 1941, Newmark, 1949, Argyris, 1960, Turner et al., 1956). Clough (1960) appears to be the first term "finite element method".

The civil engineer and structural geologists are dealing with the structures first calculates the force-displacement relationship for each element of the structure and then proceeds to assemble the whole following a well defined procedure of establishing local equilibrium at each "node" or connecting point of the structure. From such equations the solutions of the unknown displacements becomes possible.

The finite element process as a method of approximation to continuum problems, the following steps suffice to describe this approach:

(i) Divide the continuum into a finite numbers of subgroups (or elements) of simple geometry (triangles, rectangles and so on).

(ii) Select key points on the elements to serve as nodes, where conditions of equilibrium and compatibility are to be enforced.

(iii) Assume displacement functions within each element so that the displacements at each generic point are dependent upon nodal values.

(iv) Satisfy strain-displacement and stress-strain relationships within a typical element.

(v) Determine stuffiness and equivalent nodal loads for a typical element using work or energy principles.

(vi) Develop equilibrium equations for the nodes of the discretized continuum in terms of the element contributions.

(vii) Solve these equilibrium equations for the nodal displacements.

(viii) Calculate stresses at selected points within the elements.

(ix) Determine support reactions at restrained nodes if desired.

The primary disadvantage of this method is to discretization of the differential equations for which the boundary conditions are difficult to satisfy. A second disadvantage is that accuracy of the results is usually poor.

This potion have been chosen from the paper (Hayashi and Kizaki, 1972) to explain the FEM for elasticity. The numerical treatment of the geological process has already been advanced in the modern structural geology as well as in the rock mechanics. Since the geological process, however, are conspicuously slow phenomena and histories, it is required in the numerical analysis carefully to take account of the phenomena and history of the geological structure. An attempt was made in this study to analyze the stress distributions in the Nepal Himalaya region by means of FEM. In performing the FEM analysis, it is assumed that the geological materials involving in the analysis are homogeneous and perfectly elastic, although it is certain that the geological rock body must be regarded as visco-elastic body as already mentioned by Uemura, T. (1971), Ito, H.

(1972) and others. This may make the results differ from the true on certain points but it would be considered to be an approach to the better understanding of the nature.

For a typical element (Fig. 4), assuming homogeneous stress within the element, the

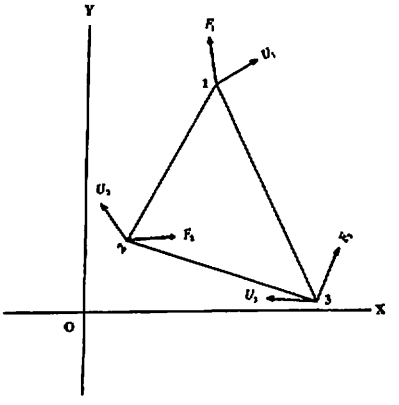

Fig. 4. A triangular finite element.

vector of nodal displacements u^e and the vector of nodal forces F^e can be express in matrix form as;

$$u^e = \begin{Bmatrix} u_1 \\ u_2 \\ u_3 \end{Bmatrix} = \begin{Bmatrix} u_{1x} \\ u_{1y} \\ u_{2x} \\ u_{2y} \\ u_{3x} \\ u_{3y} \end{Bmatrix}, \quad F^e = \begin{Bmatrix} F_1 \\ F_2 \\ F_3 \end{Bmatrix} = \begin{Bmatrix} F_{1x} \\ F_{1y} \\ F_{2x} \\ F_{2y} \\ F_{3x} \\ F_{3y} \end{Bmatrix} \tag{1}$$

By continuity of displacement within the element and with adjacent elements, a displacement function of two linear polynomials can be chosen for the case of two dimensions. So it can be represented as follows;

$$u = \begin{Bmatrix} u_x \\ u_y \end{Bmatrix} = \begin{bmatrix} a_0 & a_1 & a_2 \\ b_0 & b_1 & b_2 \end{bmatrix} \cdot \begin{Bmatrix} 1 \\ x \\ y \end{Bmatrix} \tag{2}$$

u: inner displacement vector

Eq.2 may be written in the form as;

$$u = \begin{bmatrix} 1 & x & y & 0 & 0 & 0 \\ 0 & 0 & 0 & 1 & x & y \end{bmatrix} \cdot \begin{bmatrix} a_0 \\ a_1 \\ a_2 \\ b_0 \\ b_1 \\ b_2 \end{bmatrix} = [R'] \cdot \alpha \tag{3}$$

Therefore the vector of nodal displacement is listed as a product of matrix and vector.

$$u^e = \begin{Bmatrix} R_1 \\ R_2 \\ R_3 \end{Bmatrix} \cdot \alpha = [R] \cdot \alpha \tag{4}$$

[R] : shape function matrix; α: generalized displacement vector.

Using x_i y_i for the x- and y- coordinate at the nodal point i, the shape function matrix $[R_i]$ at the point is represented by;

$$[R_i] = \begin{bmatrix} 1 & x_i & y_i & 0 & 0 & 0 \\ 0 & 0 & 0 & 1 & x_i & y_i \end{bmatrix}, \quad i = 1, 2, 3 \tag{5}$$

For eq.4 the generalized displacement vector α are given by

$$\alpha = [R]^{-1} \cdot u^e \tag{6}$$

Using Δ for $\begin{vmatrix} 1 & x_1 & y_1 \\ 1 & x_2 & y_2 \\ 1 & x_3 & y_3 \end{vmatrix}$, the inverse matrix $[R]^{-1}$ will be expressed;

$$[R]^{-1} = \frac{1}{\Delta} \begin{bmatrix} \Delta_{11} & 0 & \Delta_{21} & 0 & \Delta_{31} & 0 \\ \Delta_{12} & 0 & \Delta_{22} & 0 & \Delta_{32} & 0 \\ \Delta_{13} & 0 & \Delta_{23} & 0 & \Delta_{33} & 0 \\ 0 & \Delta_{11} & 0 & \Delta_{21} & 0 & \Delta_{31} \\ 0 & \Delta_{12} & 0 & \Delta_{22} & 0 & \Delta_{32} \\ 0 & \Delta_{13} & 0 & \Delta_{23} & 0 & \Delta_{33} \end{bmatrix} \tag{7}$$

where Δ equals to two times area of the triangle elements and Δ_{ij} is the cofactor of i, j-components of Δ , for example, $\Delta_{23} = \begin{vmatrix} 1 & x_1 \\ 1 & x_3 \end{vmatrix}$. Consequently, from eq. 3 and eq. 6 the inner displacement of the triangle is equated as follows;

$$\begin{aligned} u &= [R'] \cdot \alpha \\ &= [R'] \cdot [R']^{-1} \cdot u^e \end{aligned} \tag{8}$$

Now strain vector e is represented as;

$$\begin{aligned} e = \begin{Bmatrix} \varepsilon_x \\ \varepsilon_y \\ \gamma_{xy} \end{Bmatrix} &= \begin{Bmatrix} \dfrac{\partial u_x}{\partial x} \\ \dfrac{\partial u_y}{\partial y} \\ \dfrac{\partial u_x}{\partial x} + \dfrac{\partial u_y}{\partial y} \end{Bmatrix} \\ &= \begin{bmatrix} 0 & 1 & 0 & 0 & 0 & 0 \\ 0 & 0 & 0 & 0 & 0 & 1 \\ 0 & 0 & 1 & 0 & 1 & 0 \end{bmatrix} \cdot \alpha = [B] \cdot \alpha \\ &= [B] \cdot [R]^{-1} \cdot u^e \end{aligned} \tag{9}$$

Where the matrix [B] is called the strain-generalized displacement matrix and its components are not functions of variables x and y, so that one can see that the strain is constant in each element.

The relation of stress vector **p** and strain vector e is;

$$P = \begin{Bmatrix} \sigma_x \\ \sigma_y \\ \tau_{xy} \end{Bmatrix}$$

$$= \frac{E(1-\nu)}{(1+\nu)(1-2\nu)} \begin{bmatrix} 1 & \frac{\nu}{1-\nu} & 0 \\ \frac{\nu}{1-\nu} & 1 & 0 \\ 0 & 0 & \frac{1-2\nu}{2(1-\nu)} \end{bmatrix} \cdot e \qquad (10)$$

$$= [K] \cdot e$$

Where ν is the Poisson's ratio, E is the Young's modulus and [K] is the stress-strain matrix. Eq. 10 is valid for the case of plane strain.

Let the virtual displacement be u^{*e} when the element is deformed, the strain energy U of this element is given by;

$$U = \int_v (e^*)^T \cdot p \, dV$$

$$= \int_v (e^*)^T \cdot [K] \cdot e \, dV$$

$$= \int_v (u^{*e})^T \cdot ([R]^{-1})^T \cdot [B]^T \cdot [K] \cdot [B] \cdot [R]^{-1} \cdot u^e \, dV$$

$$= \int_v (u^{*e})^T \cdot [B^*]^T \cdot [K] \cdot [B^*] \cdot [R]^{-1} \cdot u^e \, dV$$

where $[B^*]$ is equal to $[B^*][R]^{-1}$ and e^* is the vector of virtual strain.

As the nodal forces are already defined by eq. 1, the external work is:

$$W = (u^{*e})^T \cdot F^e$$

And the strain energy is equal to the external work, so that the following equation holds.

$$(u^{*e})^T \cdot F^e = \int_v (u^{*e})^T \cdot [B^*]^T \cdot [K] \cdot [B^*] \cdot u^e \, dV$$

$$= (u^{*e})^T \{ \int_v [B^*]^T \cdot [K] \cdot [B^*] dV \} \cdot u^e$$

While the vector of nodal force is represented by;

$$F^e = \left\{ \int_v [B^*]^T \cdot [K] \cdot [B^*] dV \right\} \cdot u^e$$

Now, the stiffness equation is obtained.

$F^e = [\Lambda] \cdot u^e$ where Λ is called the stiffness matrix and can be written in the form;

$$\Lambda = \left\{ \int_v [B^*]^T \cdot [K] \cdot [B^*] dV \right\}$$

In this case, each matrix is constant in the element, then the product of matrices i.e. $[B^*]^T \cdot [K] \cdot [B^*]$, is constant. Consequently, it is possible to take off the integral mark, $\Lambda = [B^*]^T \cdot [K] \cdot [B^*] \cdot V$, where V is the volume of the element.

By solving the above stiffness matrix, one can get undecided nodal forces and nodal displacements for every element. Moreover, using these nodal displacements, the values of stress and strain could be obtained. Further and detailed discussions on FEM are referred to such publications as Zienkiewicz et al. (1967) and so forth.

2.2 Modeling

Four different cross sections are used to justify the effect of material properties of rock formations applied on these cross sections. Referring papers which were published during 1979 to 1999, we have selected these cross sections for four models to verify the adequate stress distribution and fault development among the models. The four cross sections are typical for the profile of Nepal Himalaya.

2.2.1 Physical properties

The following cross-sections have been used in the present study:

(i) Model - 1

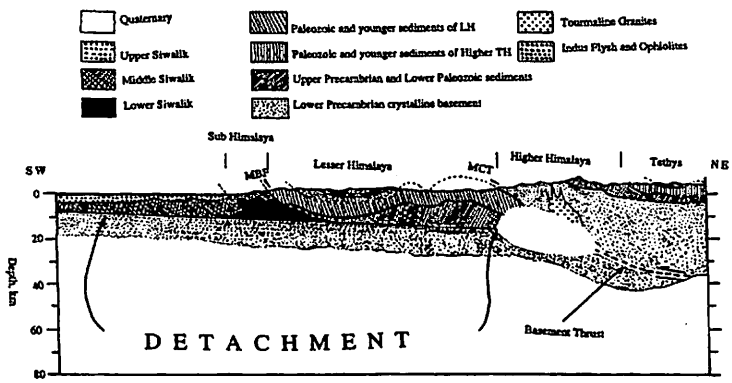

Fig. 5. Cross section of the central Himalaya are shown with geology. Modified from Seeber et al. (1980) and the surface geology is from Gansser (1964).

(ii) Model - 2

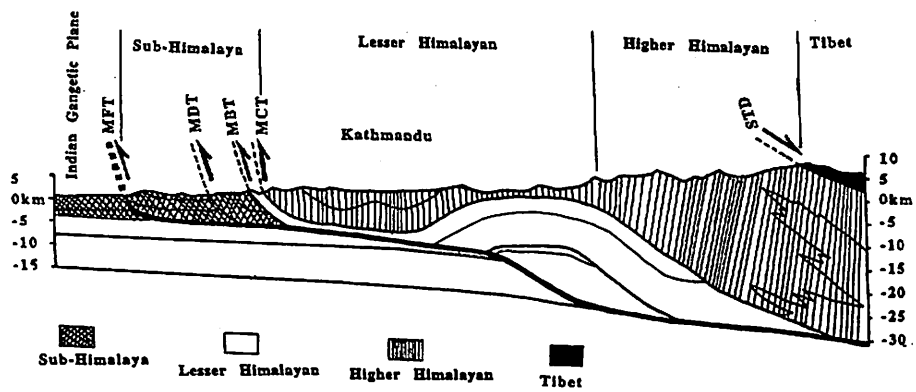

Fig. 6. Geological section across the central Himalaya of Nepal. Modified from Brunel (1986), Pandey et al. (1999).

(iii) Model - 3 (A)

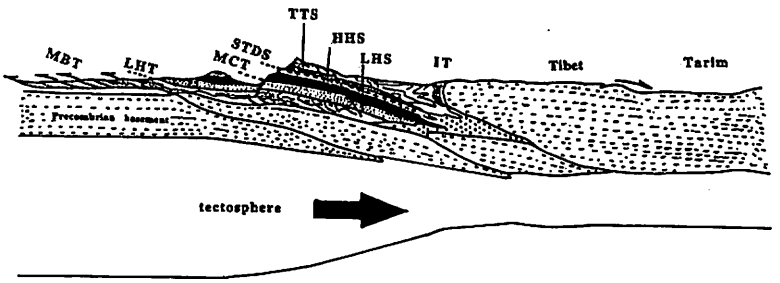

Fig. 7. Present stage of the geological cross section for the tectonic evalution of the Himalayan Metamorphic belt in central Nepal. Modified from Kaneko (1997).

(iv) Model - 3 (B)

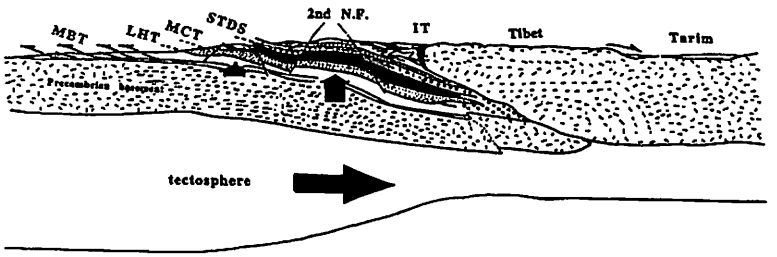

Fig. 8. Mountain building stage (5-11 Ma) of the geological cross section for the tectonic evalution of the Himalayan Metamorphic belt in central Nepal. Modified from Kaneko (1997).

The geometry of all the cross-sections are more or less same although each has been taken from different phenomenon. It is difficult to distinguish the rocks belonging to the layer according to their geological meaning. A number of rocks belong to the layers can be selected in the following formula

$$\binom{n}{c}_{k} = \frac{n!}{k!\,(n-k)!} \qquad (1)$$

where n is the number of rocks belonging to the layer and k is the number of layer ($n>k$).

The following tables are showing the material properties for different models

Table 2. Material properties of Model - 1

Stratigraphic unit	Layer	Lithology	Poisson's ratio	Density (kg/m^3)	Young's Modulus (GPa)	Friction angle (degree)	Cohesion (MPa)
Sub Himalaya	6	Sandstone, Siltstone, Mudstone	0.25	2500	40	35	18
Lesser Himalaya	4	Sandstone, Limestone	0.30	2700	70	50	17
Higher Himalaya	5	Marbel, Granite, Limestone	0.35	2900	80	58	10
Tethys Himalaya	1, 2, 3	Sandstone, Impure limestone	0.25	2600	50	45	20

Table 3. Material properties of Model - 2

Stratigraphic unit	Layer	Lithology	Poisson's ratio	Density (kg/m^3)	Young's Modulus (GPa)	Friction angle (degree)	Cohesion (MPa)
Sub Himalaya	3	Sandstone, Siltstone, Mudstone	0.25	2500	40	35	18
Lesser Himalaya	2	Sandstone, Limestone	0.30	2800	70	50	17
Higher Himalaya	1	Marbel, Granite, Limestone	0.35	2900	80	58	10
Tethys Himalaya	4	Sandstone, Impure limestone	0.25	2600	50	45	20

Table 4. Material properties of Model - 3 (A & B)

Stratigraphic unit	Layer	Lithology	Poisson's ratio	Density (kg/m^3)	Young's Modulus (GPa)	Friction angle (degree)	Cohesion (MPa)
Sub Himalaya	2	Sandstone, Siltstone, Mudstone	0.25	2600	40	35	18
Lesser Himalaya	3	Sandstone, Limestone	0.30	2600	60	48	15
Higher Himalaya	4	Gneiss Granite, Limestone	0.35	2900	80	50	17
Tethys Himalaya	5	Sandstone, Impure limestone	0.25	2600	50	45	20
Granitic Layer	1	Granite, Marbel Limestone	0.35	2900	80	58	10

2.2.2 Boundary Condition

In all models the upper surface is free to deform horizontally and vertically. The lower boundary is restricted to move vertically but allowed to deform horizontally. The nodes at the left boundary can move only vertically. The node at the joining of lower and the left boundary is fixed. SW (south west) to NE (north east) horizontal shortening up to 375 m is applied in incremental steps of 75 m, equally divided over the cross-section. Model - 1 contains 352 nodes, 564 elements and the material properties are shown in Table 2; model - 2 contains 501 nodes, 884 elements and the material properties are shown in Table 3; model - 3 (A & B) contains 353 nodes, 624 elements, and 491 nodes, 880 elements respectively and the material properties are shown in Table 4.

According to the rules described above, the boundary conditions for all the models are as follows:

Model - 1: For the nodes 1, 2 and 3 displacement along horizontal direction is only permitted; node no. 346, 347, 348, 349, 350, 351 are permitted to move only vertically; node no. 352 is restricted to move to all directions; node no. 6,

9, 12, 15, 19, 23, 27, 31, 35, 39, 43, 47, 51, 55, 59, 63, 73, 78, 88, 95, 105, 111, 120, 125, 133, 140, 147, 154, 160, 174, 183, 188, 196, 200, 204, 208, 212, 219, 224, 237, 242, 248, 254, 259, 260, 265, 272, 284, 304, 315 and 326 can move horizontally and vertically (Fig. 9). Other nodes are free.

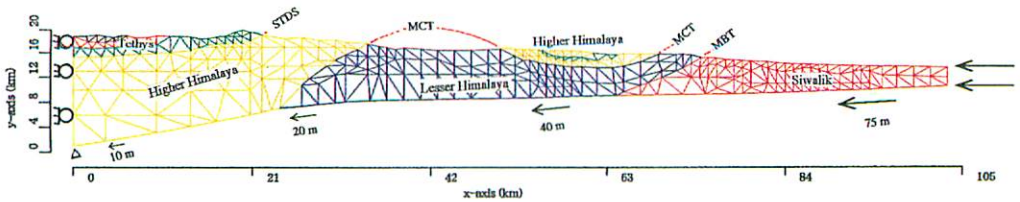

Fig. 9. Boundary condition of model - 1. It contains 352 nodes and 564 elements. The lower boundary is restricted to move vertically but allowed to deform horizontally. The nodes at the left boundary can move only vertically. The node at the joining of lower and the left boundary is fixed. SW (south west) to NE (north east) horizontal shortening up to maximum 375 m (equivalent displacement at 7.5 cm/yr of 5000 yr) is applied in incremental steps of 75 m, at the southwestern end of the cross section.

Model - 2: For node no. 1, 2, 3, 4, 5, 6, 7 and 8 deformation takes place along horizontal direction only; node no. 16, 17, 32, 33, 34, 50, 51, 74, 75, 91, 92, 102, 103, 123, 124, 166, 167, 187, 188, 206, 239, 240, 264, 265, 296, 297, 314, 316, 347, 348, 366, 368, 382, 383, 406, 407, 413, 414, 439, 441, 442 and 465 can move horizontally and vertically; node no. 466 is forbidden to move to all directions; node no. 467, 468, 469, 486, 487, 488, 489, 490, 501 and 500 can move only vertical direction; other nodes are free to move to all directions (Fig. 10).

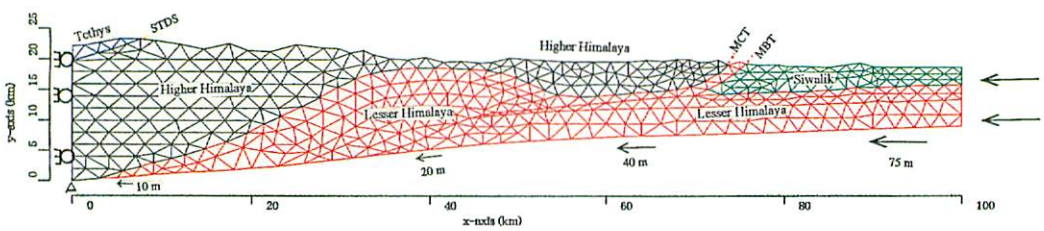

Fig. 10. Boundary condition of model - 2 which contains 501 nodes and 884 elements. The lower boundary is restricted to move vertically but allowed to deform horizontally. The nodes at the left boundary can move only vertically. The node at the joining of lower and the left boundary is fixed. SW (south west) to NE (north east) horizontal shortening up to maximum 375 m (equivalent displacement at 7.5 cm/yr of 5000 yr) is applied in incremental steps of 75 m, at the southwestern end of the cross section.

Model - 3(A): For node no. 1, 2, 3, 4, 5 and 6 deformation takes place along horizontal direction only; node no. 17, 18, 40, 41, 57, 69, 70, 84, 106, 107, 118, 119, 135, 136, 157, 158, 180, 206, 207, 261, 262, 284, 285 and 307 can move horizontally and vertically; node no. 353 is forbidden to move to all directions; node no. 343, 344, 345, 346, 348, 350, 351 and 352 can move only vertical direction; other nodes are free to move to all directions (Fig. 11).

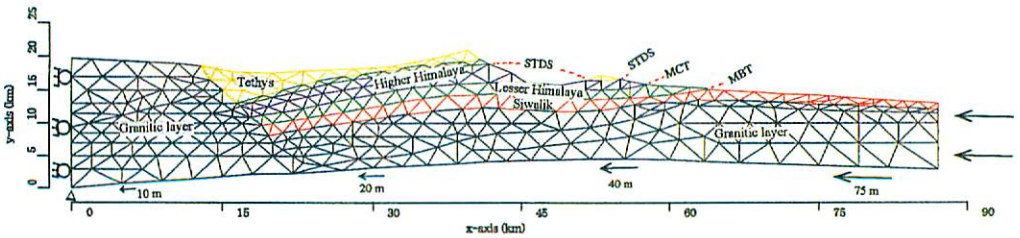

Fig. 11. Boundary condition of model - 3(A). It contains 353 nodes and 624 elements. The lower boundary is restricted to move vertically but allowed to deform horizontally. The nodes at the left boundary can move only vertically. The node at the joining of lower and the left boundary is fixed. SW (south west) to NE (north east) horizontal shortening up to maximum 375 m (equivalent displacement at 7.5 cm/yr of 5000 yr) is applied in incremental steps of 75 m, at the southwestern end of the cross section.

Model - 3(B): For node no. 1, 2, 3, 4, 5 and 6 deformation takes place along horizontal direction only, node no. 12, 13, 26, 27, 57, 58, 78, 79, 81, 96, 97, 114, 115, 134, 135, 157, 158, 209, 210, 231, 232, 252, 253, 273, 274, 331, 332, 334, 335, 340, 341, 351, 354, 356, 415, 416, and 417 can move to both horizontal and vertical direction; 442 is forbidden to move to all directions; node no. 443, 463, 464, 465, 479, 480, 481, 488, 489, and 491 can move only vertical direction; other nodes are free (Fig. 12).

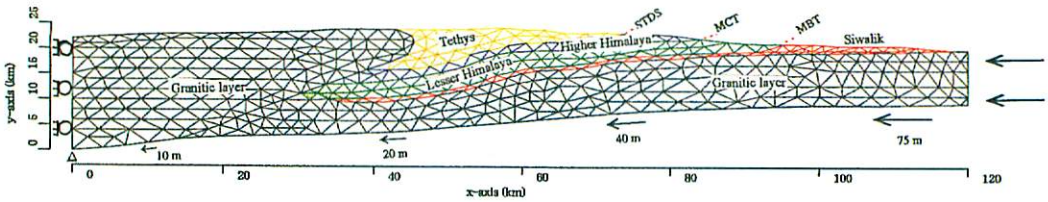

Fig. 12. Boundary condition of model - 3(B) which have 491 nodes and 880 elements. The lower boundary is restricted to move vertically but allowed to deform horizontally. The nodes at the left boundary can move only vertically. The node at the joining of lower and the left boundary is fixed. SW (south west) to NE (north east) horizontal shortening up to maximum 375 m (equivalent displacement at 7.5 cm/yr of 5000 yr) is applied in incremental steps of 75 m, at the southwestern end of the cross section.

2.2.3 Criterion for Selection of Displacement Boundary Condition

Marine geophysical data from the Atlantic and Indian Oceans allow reconstruction of India and Eurasia for the last 70 Ma. A rapid decrease in convergence from about 100 mm/yr to 50 mm/yr occurred approximately 40 Ma ago, approximately or slightly later than the date inferred geologically for the collision. The Himalayan mountain originated as a result of collision between the Indian and Eurasian plates. The Indian plate converges northward at an average rate of 50 mm/yr and is underthrusting beneath Tibet (Thakur et al., 2000). Of the total convergence, ~20 mm/yr (Lave & Avouac, 1998; Bilham et al., 1997) is accommodated across the Himalaya and the remaining convergence is taken up farther north (Peltzer & Saucie, 1996; Yeats & Thakur, 1998).

Taking the estimate that 300 to 400 km of shortening has occurred in the Himalaya (Gansser, 1966; Mattauer, 1975; Warsi & Molnar, 1977) and assuming that underthrusting began in the Oligocene or late Eocene (Gansser, 1964; Hamet & Allegre, 1976), the average rate of shortening is about 10 mm/yr. This rate is consistent with the rate of 10-20 mm/yr inferred from releveling data of Chugh, 1974, with geodetic measurements across one fault (Sinval et al., 1973), and from seismic moments of earthquakes (Chen & Molnar, 1977). All of the rates are substantially less than the convergence between India and Eurasia for the last 10 Ma (Le Pichon, 1968; Minster et al., 1974). The Himalaya, therefore, seem to absorb only fraction of the convergence; the remainder occurs apparently by deformation of the part of Asia north of the Himalaya (Molnar & Tapponnier, 1975).

Hayashi (1987, 1988 and 1992) numerically simulated the uplift of the Tibetan plateau and the Himalayas assuming that the northerly migration of the Indian plate deforms the overlying Asian continental crust which behaves as an incompressible Newtonian fluid of Asia above the rigid upper mantle. In these models, the Newtonian sialic crust is deformed by a 60 km deep ramp dipping 45 degrees northwards in a rigid mantle asthenosphere moving at 100 mm/yr.

Gathering our knowledge and improve our skillness, 3 cm/yr, 5 cm/yr, 7.5 cm/yr and 10 cm/yr displacement had been applied for all the models. Considering all the cases mentioned above, 7.5 cm/yr displacement have been taken for the present analysis.

Procedure for obtaining input and out put data

Primarily based on the seismic cross-section but also incorporating field data, a 2 dimensional finite element model has been constructed. The elements used are three-nodes, triangles (Fig. 4), with linear shape functions and thus constant strain and stress. The finite element code used for the elastic calculation is *elas.f*.

To produce input data, the cross-sections are divided into triangle elements for identifying the coordinates of the nodal points and imposing the boundary conditions according to the structural and tectonic environment.

Input data can be made manually using section paper or the tablet mechanism under Macintosh computer system. It is important to note that to let the x-axis and y-axis in the cross-section be parallel to the frame sides of the tablet as much as possible. Then using the tablet the coordinates of all the nodes will be obtained. Therefore, after getting the coordinates of all nodes, the determination of element connection data will be made manually. Based on the coordinates of the nodes, a simple profile map with the same scale of x-axis and y-axis can be drawn by using a Fortran program (*net.func*). After that the input data will be obtained finally.

We can verify the shape of the model with the cross section. If some thing wrong with the cross section, it will be easily located by the soft *net.func*.

After getting the input data, finite element method programs, *elas.f*, *band.f* and

net.func written in Fortran are applied to obtain the stress field of all the models. Program *net.func* is used to show the geometrical structure of the cross-section under triangles only. Program *band.f* is used to determine the highest value of the difference among the nodes of respective triangles. After computing, *ibw* (the highest difference) is obtain and is unique. Computing time depends on the value of the ibw. If *ibw* is large, computing time will be long. Program *elas.f* is used to compute the stress field of the model. In this program, boundary condition file, material properties and data files are used to simulate the maximum principal stress (σ_1) and minimum principal stress (σ_2). Using the principal stresses, a soft ware (*stress.func*) can be applied to find out the stress distribution which identifies the deformation pattern along the region.

3. Result

In the numerical experiments presented in this study, the fault distribution and stress pattern are described by two parameters: displacement boundary condition and, cohesion and friction angle. The numerical experiments show that acceptable distribution of deformation can be calculated for some choice of displacement boundary condition (75 m/1000yr, 150 m/2000yr, 225 m/3000yr, 300 m/4000yr, and 375 m/5000yr) and also for the values of cohesion strength and friction angle. A general discussion is made for all the models analyzing the points mentioned above of the Himalaya under FEM.

3.1 Model - 1

Horizontal displacement is 75 m/1000 yr. (*Fig. 13*): Principal stresses are stronger in the deeper portion than the shallower one. Maximum principal stresses are distributed near vertically while minimum principal stresses are distributed near horizontally all over the region. Hydrostatic condition occurs below the Tethys Himalaya that belongs to 6 to 12 km depth of the Higher Himalaya. Left side of the upper half of MCT and MBT, σ_1 is distributed horizontally but vertically at the right side. Principal stresses are compressive along all the region. In the shallower part of the Siwalik and the Tethys, principal stresses are very small (near about 0). The values of compressive σ_1 are from 0 to 450 MPa (element no. 541) and the values of compressive σ_2 are from 0 to 350 MPa (element no. 418).

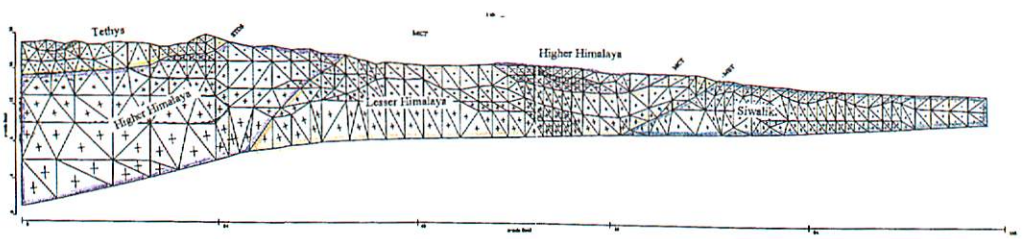

Fig. 13. Stress distribution of model - 1. 75 m displacement boundary condition is subjected to the bottom of the model during 1000 year.

Horizontal displacement is 375 m/5000 yr. (*Fig. 14*): Principal stresses are stronger in the deeper portion than the shallower one. Maximum principal stresses are distributed horizontally and minimum principal stresses are distributed vertically all over the region. Hydrostatic condition occurs beneath the deeper part of the Higher Himalaya, that is near the MCT and bounded by lower boundary. Principal stresses are compressive along all the region except element no. 237, 248 and 249. These elements show negligible extensive stress (less than 100 MPa) field. In the shallower part of the Siwalik and the Tethys area, minimum principal stresses are very small (near about 0). The limits for σ_1 are from 40 MPa (element no. 442) to 1.1 GPa (element no. 418) and from 0 to 500 MPa (element no. 418) for σ_2.

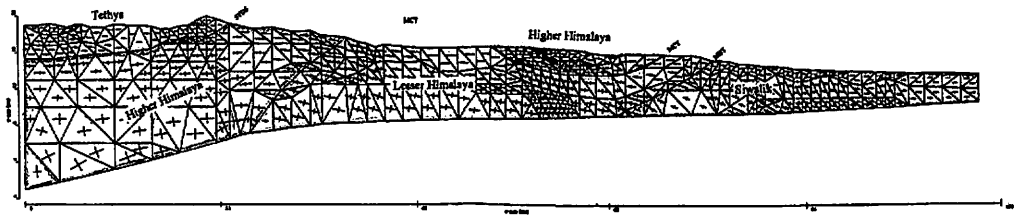

Fig. 14. Stress distribution of model - 1. 375 m displacement boundary condition is subjected to the bottom of the model during 5000 year. Red blocks indicating extensive stress field.

3.2 Model - 2

Horizontal displacement is 75 m/1000 yr. (*Fig. 15*): Principal stresses are stronger in the deeper portion than the shallower one. Maximum principal stresses are distributed near vertically but minimum principal stresses are distributed near horizontally over all the region. Hydrostatic condition appears below the Tethys Himalaya that belongs to 5 to 10 km depth of the upper part of the Higher Himalaya and some parts of the Siwalik and the Lesser Himalaya along the boundary between them. Along the shallower part of the Higher Himalaya, Lesser Himalaya and the Siwalik, σ_1 is distributed horizontally where σ_2 is very small (near 0.0 MPa). Principal stresses are compressive along all the region. The limits of compressive σ_1 are from 30 MPa (element no. 289) to 630 MPa (element no. 825) and σ_2 are from 0 to 390 MPa (element no. 792, 825, 826 and 827).

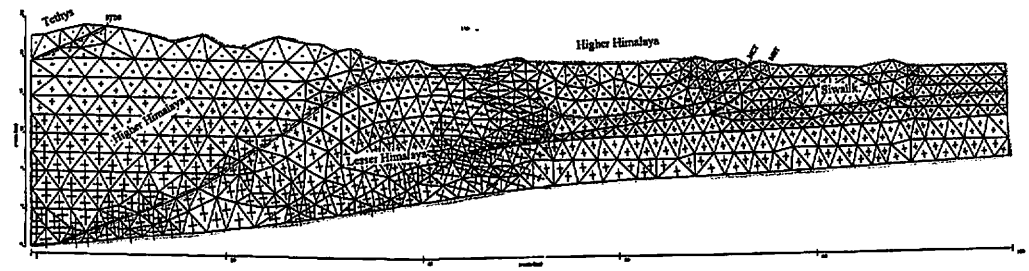

Fig. 15. Stress distribution of model - 2. 75 m displacement boundary condition is subjected to the bottom of the model during 1000 year.

Horizontal displacement is 375 m/5000 yr. (Fig.16): Principal stresses are stronger in the deeper portion than the shallower one. Maximum principal stresses are distributed horizontally and minimum principal stresses are distributed vertically all over the region. Hydrostatic condition occurs in the dipper part of the Higher Himalaya, and some parts of the Lesser Himalaya along the deeper part of the MCT and MBT region. Principal stresses are compressive along all the region except element no. 251, 256, 440, 476, 661, and 663. These elements show negligible extensive stress (less than 100 MPa) field. In the shallower part of the Siwalik and the Tethys area, minimum principal stresses are very small (near about 0). The limits for σ_1 are from 90 MPa (element no. 871) to 680 MPa (element no. 820) and from 0 to 650 MPa (element no. 819) for σ_2.

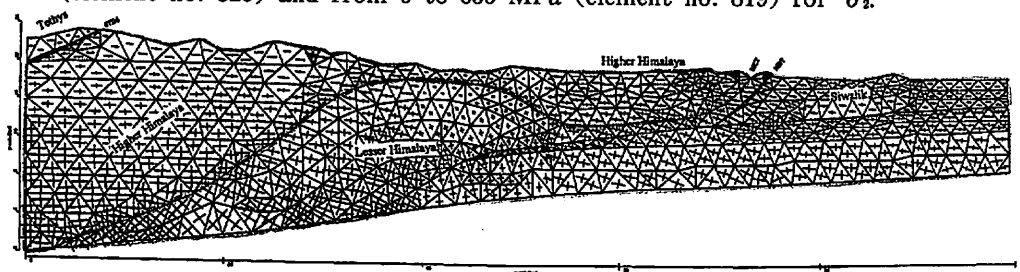

Fig. 16. Stress distribution of model - 2. 375 m displacement boundary condition is subjected to the bottom of the model during 5000 year. Red blocks indicating extensive stress field.

3.3 Model - 3 (A) (Present stage)

Horizontal displacement is 75 m/1000 yr. (Fig 17): Principal stresses are stronger in the deeper portion than the shallower one. Along the Siwalik region, σ_1 is distributed horizontally (Gangatic plane) where as in the deeper part it is distributed near vertically. In the Lesser Himalaya, σ_1 tends to horizontal to vertical direction along the shallower part to deeper part. In the Higher Himalaya σ_1 shows the same tendency as the Siwalik and the Lesser Himalaya but the deeper most part obtaining hydrostatic condition. Along all the regions of the Tethys Himalaya, σ_1 is distributed horizontally. Most of the area of the Granitic layer σ_1 is distributed near vertically but σ_2 is near horizontal except the part just below the Siwalik region, where σ_1 is distributed horizontally. Hydrostatic condition occurs in some parts of the Granitic layer. Principal stresses are compressive along all the region. The limits of compressive σ_1 are from 30 (element no. 283) to 530 MPa (element no. 305) and σ_2 are from 0 to 340 MPa (element no. 526).

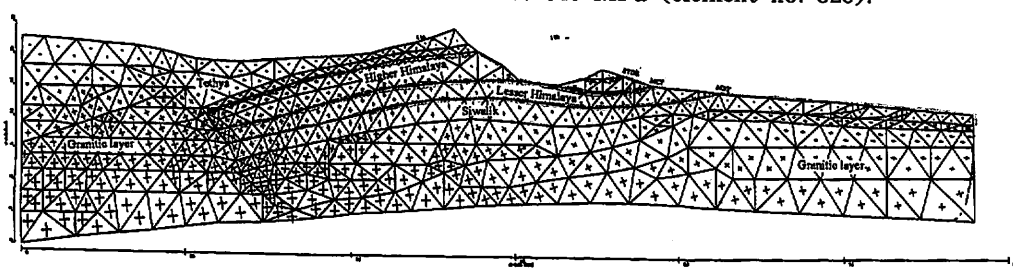

Fig. 17. Stress distribution of model - 3(A). 75 m displacement boundary condition is subjected to the bottom of the model during 1000 year.

Horizontal displacement is 375 m/5000 yr. (Fig. 18): Principal stresses are stronger in the deeper portion than the shallower one. Maximum principal stresses and minimum principal stresses are distributed almost horizontally and vertically, respectively over all the region but hydrostatic condition is observed along the deeper part of Higher Himalaya, Lesser Himalaya, and some parts of Granitic layer. Principal stresses are compressive along all the region except element no. 163, 187 and 190. These elements show negligible extensive stress (less than 100 MPa) field The limits for σ_1 are from 40 (element no. 283) to 740 MPa (element no. 529) and from 0 to 490 MPa (element no. 572) for σ_2.

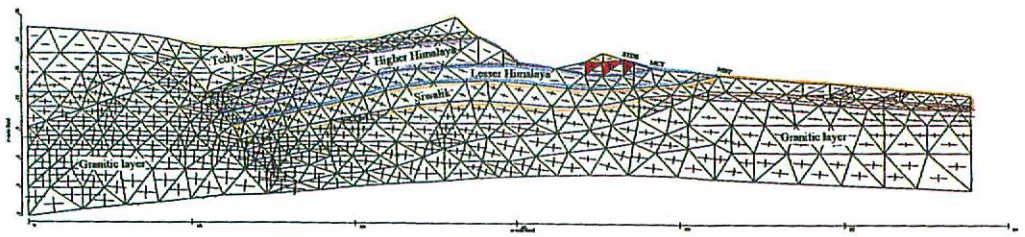

Fig. 18. Stress distribution of model - 3(B). 375 m displacement boundary condition is subjected to the bottom of the model during 5000 year. Red blocks indicating extensive stress field.

3.4 Model - 3 (B) (Mountain building stage)

Horizontal displacement is 75 m/1000 yr. (Fig. 19): Principal stresses are more stronger in the deeper portion than the shallower one. Along the Siwalik region, σ_1 is distributed horizontally (Gangatic plane) where as in the deeper part it is distributed vertically. In the Lesser Himalaya, σ_1 tends to horizontal to vertical direction along the shallower part to dipper part. In the Higher Himalaya σ_1 shows the same tendency as the Siwalik and the Lesser Himalaya but the dipper most part obtaining hydrostatic condition. In the Tethys Himalaya, σ_1 is distributed horizontally along the shallower part but the deeper part shows near vertical direction. Shallower part of the Granitic layer, σ_1 shows horizontal direction while in the deeper it shows vertical direction. Hydrostatic condition occurs in some places of the Granitic layer. Principal stresses are compressive along all the regions. The limits of compressive σ_1 are from 20 (element no. 45) to 590 MPa (element no. 723) and σ_2 are from 0 to 420 MPa (element no. 719).

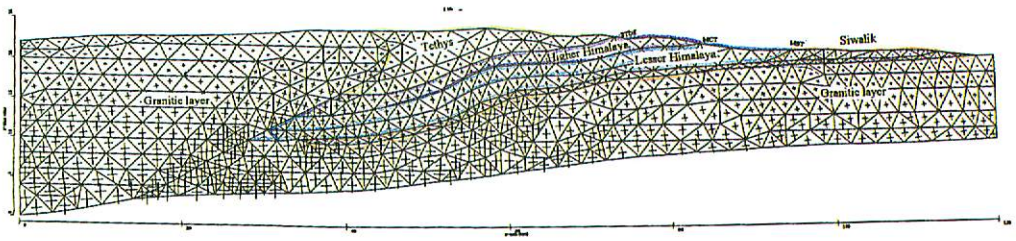

Fig. 19. Stress distribution of model - 3(B). 75 m displacement boundary condition is subjected to the bottom of the model during 1000 year.

Horizontal displacement is 375 m/5000 yr. (Fig. 20): Principal stresses are more stronger in the deeper portion than the shallower one. σ_1 and σ_2 are distributed horizontally and vertically, respectively all over the region except along the deeper part of the Granitic layer, where obtaining reverse distribution of σ_1 and σ_2. Hydrostatic condition is observed along the deeper part of Higher Himalaya, Lesser Himalaya, and some parts of Granitic layer. Principal stresses are compressive along all the regions except element no. 521. This element shows negligible extensive stress (less than 100 MPa) field. The limits for σ_1 are from 100 (element no. 66) to 880 MPa (element no. 719) and from 0 to 640 MPa (element no. 719) for σ_2.

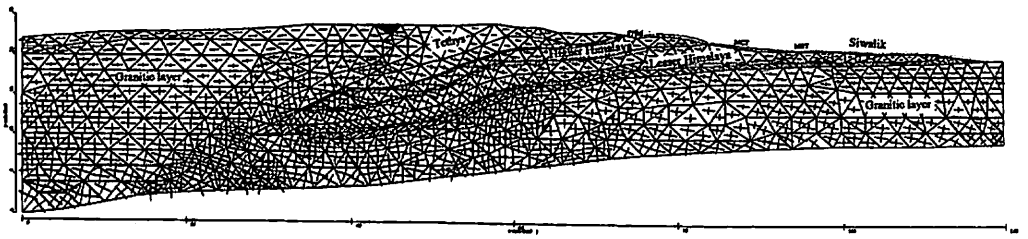

Fig. 20. Stress distribution of model - 3(B). 375 m displacement boundary condition is subjected to the bottom of the model during 5000 year. Red blocks indicating extensive stress field.

4. Discussion

4.1 Seismicity and Focal Mechanism Solution

Himalaya is seismically active attests to current tectonic activity. Four earthquakes with magnitude more than 8 occurred since 1897 and all appear to be related to mountain building processes in the Himalaya. Although earthquakes occur in neighboring regions, a belt of seismicity follows the range along the entire length. According to International Seismological Center and the International Oceanic and Atmospheric Administration for the period 1961-1970, most of the epicenters fall near the trace of the MCT and not the MBF. From this, it is tempting to conclude that the MCT is active but not the MBF. However, when one considers that the MBF dips gently to the north or northeast (Gansser, 1964), and that the earthquakes occur at finite depth, it seems more reasonable to conclude that along most of the Himalaya, the activity is associated with MBF and the Zone surrounding it.

The seismicity at both ends of the Himalaya appears to be more complicated with diffuse zones south of main range. In the east, seismicity is distributed over the Shillong plateau and it's margins (Fig. 21). In the northwest, using a dense network of stations, Arambruster et al., (1976) and Jacob et al., (1976) located earthquakes in a broad area from 50 km north of the MCT to 150 km south of it and extending to depths greater than 60 km. They consider both the MCT and the MBF to be active, and in fact used the earthquake epicenters to map the westward continuation of the MBF beyond where it is

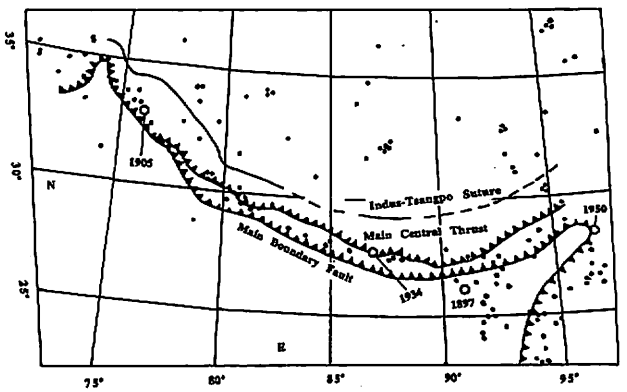

Fig. 21. Shallow focus seismicity of the Himalaya region. Selected well located epicenters from ISC or NOAA from 1961-1970 and major shocks since 1897 (Molnar et al., 1977).

recognized geologically. Although the tectonics of this segment of the Himalaya is probably more complicated than to the southeast, the lesson to be learned is probably that seismicity along the entire range is not restricted to a single narrow fault zone.

Several published studies of focal mechanism solutions of earthquakes in the Himalaya region give the same general pattern of thrust faulting, with one plane dipping gently beneath the Himalaya (Armbruster et al., 1976; Banghar, 1974; Ben Menahen et al., 1974; Chen & Molnar, 1977; Fitch, 1970; Ichikawa et al., 1972; Molnar et al., 1973; Rastogi et al., 1973; Tandon, Srivastava, 1975). Among these studies slightly different approaches have been taken, and in a few cases, different solutions for the same earthquake were reported, but the general pattern is observed for nearly all. Except possibly for the 1950 Assam earthquake all ten of the focal mechanism solutions for events in the Himalaya show large components of thrusting (Fig. 22). Assuming that dips approximately north

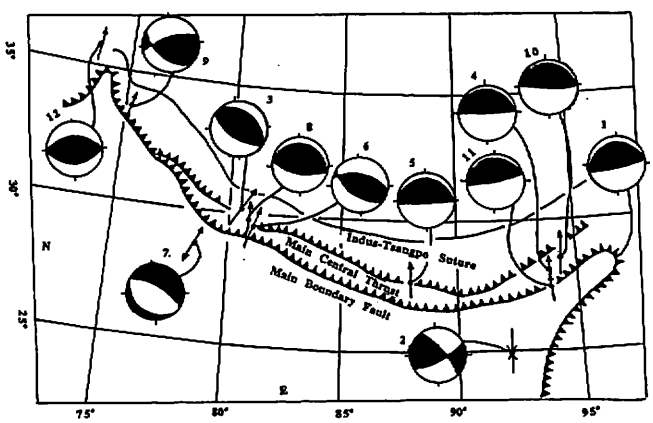

Fig. 22. Focal mechanism solutions. Single arrows show presumed direction on underthrusting. Opposing arrows for event 2 show approximate direction of maximum compression and diverging arrows for event 7 show approximate direction of least compression. Numbers correspond to table 5. Circes show lower hemisphere plots of focal sphere - dark areas represent quadrant with compressional first arrivals (Molnar et al., 1977).

or northeast is the fault plane, the slip vectors are fairly well determined and show an underthrusting to the north or northeast. The dips of the fault planes appear to be shallower for earthquakes in the southeast portion of the Himalaya than elsewhere. The solutions are based on first motions of p waves and, when possible, s waves, from recordings of long period seismograms. Parameters for these solutions are given in Table 5.

Table 5. Catalog of focal mechanism solution parameters

NO	Earthquake date	Lat (N)	Long(E)	Pole		Pole		Pole		T-axis		B-axis	
				Az.	pl.	Az.	pl.	Az.	pl.	Az.	pl.	Az.	pl.
01	15 AUG 1950	28.50	96.70	351	12	171	78	171	33	351	57	81	0
02	19 JUN 1963	24.97	92.06	235	20	330	16	192	5	287	24	91	60
03	26 SEP 1964	29.96	80.46	40	30	220	60	220	15	40	75	135	0
04	21 OCT 1964	28.04	93.75	357	5	177	85	177	40	357	50	87	0
05	12 JAN 1965	27.40	87.84	0	15	180	75	180	30	0	60	90	0
06	27 JUN 1966	29.62	80.83	36	41	196	49	207	4	94	86	297	10
07	15 MAR 1966	28.17	78.93	42	59	222	31	222	76	42	14	132	0
08	16 DEC 1966	29.62	80.79	190	66	10	24	190	21	10	69	100	0
09	20 FEB 1967	33.63	75.33	168	25	42	50	10	14	123	57	272	28
10	14 MAR 1967	28.41	94.29	3	10	183	80	183	35	3	55	93	0
11	19 FEB 1970	27.40	93.99	347	5	167	85	167	40	347	50	77	0
12	03 SEP 1972	35.98	73.42	0	50	180	40	0	5	180	50	90	0

Azimuth (Az.) and plunges (pl.) are given for poles of each possible nodal plane and for P, T, and B axis, which roughly approximate the directions of maximum, minimum and intermediate compressive stresses.

In northern Pakistan, where focal mechanism solutions of smaller earthquakes have been examined in detail (Arambruster et al., 1976, Jacob et al., 1976), the same basic pattern prevails but greater complexity. The seismicity also scatters at the eastern end of the Himalaya near the Shillong plateau. A poorly determined solution was obtained for a small event (June 19, 1963) near the Dauki fault (Evens, 1964), which separates the crystalline rocks of the Shillong plateau from the Cenozoic sediments south of it. Drilling data suggest as much as 250 km of right lateral strike slip motion on this fault (Evans, 1964).

The August 15, 1966 earthquake occurred 100 km southwest of Himalayan front, the Ganga Basin. Normal faulting occurred on a plane that strikes approximately parallel to the Himalaya. The interpretation that Stauder (1968), Isacks, Oliver, Sykes (1968) gave, that the normal faulting is due to a stretching of the upper part of the lithosphere as it bends down at the trench. Menke & Jacob (1976) located many earthquakes beneath the Ganga basin and south of it. In this sense the 1966 earthquake is not unusual (Molnar et al., 1979).

4.2 Mohr-Coulomb failure envelope

Mohr-Coulomb failure envelope is a method which helps to identify the location of

fault plane within the crust or in the surface. Since FEM helps to compute the 2D stress field (σ_1 and σ_2) under *elas.f* program for all the models, the third unknown principal stress (σ^*) can be obtained by using the equation

$$\sigma^* = \nu(\sigma_1 + \sigma_2) \quad (12)$$

where, ν is Poisson's ratio (Timoshenko & Goodier, 1970, Hayashi and Kizaki, 1972), σ_1 and σ_2 (calculated by FEM) are the principal stresses. After getting the values of σ_1, σ_2 and σ^* for each element, it is easy to compute which principal stresses, σ_1, σ_2, and σ^* are the maximum, intermediate and minimum. According to the order of magnitude, a newly defined stress field can be obtained by using the newly obtained principal stresses σ_1, σ_2 and σ_3.

The Mohr-Coulomb failure envelope is shown in Fig. 23. It is based on a linear

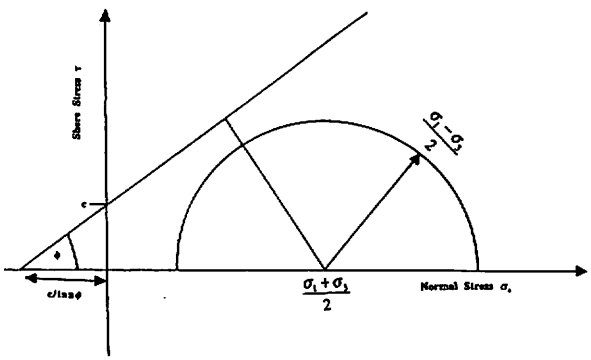

Fig. 23. Mohr circle construction demonstrating the concept of proximity to failure.

relationship between the share stress τ and the normal stress σ_n:

$$\tau_{failure} = c + \sigma_n \tan\phi \quad (13)$$

where c is the cohesive strength of the rock and ϕ is the angle of internal friction. Failure occurs when the Mohr circle first touches the failure envelope. This occurs when the radius of the Mohr circle, $\frac{\sigma_1 - \sigma_3}{2}$, is equal to the perpendicular distance from the center of the circle at $\frac{\sigma_1 + \sigma_3}{2}$ to the failure envelope,

$$\left(\frac{\sigma_1 - \sigma_3}{2}\right)_{failure} = c\cos\phi + \left(\frac{\sigma_1 + \sigma_3}{2}\right)\sin\phi \quad (14)$$

As the newly defined stress field of each model is available, it is possible to locate in which element, fault will be developed according to Mohr circle.

The proximity to failure P_f , can be defined as the ratio between the actual radios of the Mohr circle, $\frac{\sigma_1 - \sigma_3}{2}$, and the radios at failure,

$$P_f = \left(\frac{\left(\frac{\sigma_1 - \sigma_3}{2}\right)}{\left(\frac{\sigma_1 - \sigma_3}{2}\right)_{failure}} \right) \quad (15)$$

One can evaluate whether faulting develops in certain element according to the value of the parameter P_f. Whenever the value of $P_f<1$, the stress state is within the failure envelope (i.e., no fault develops), but when $P_f \geq 1$, failure occurs. Thus P_f is taken as an indicator to define whether the fault develops or not. Using the eq. (15) it is easy to find out the location of failure element.

Some experiments have done for choosing the material properties according to the layer using eq. (11). Table 2-4 show the required material properties for our numerical modeling. We have imposed some boundary conditions like 3 cm/yr, 5 cm/yr, 7.5 cm/yr and 10 cm/yr; among these we describe only 7.5 cm/yr during 1000 to 5000 yr period. According to the boundary condition 75 m/1000yr, the average limits for σ_1 and σ_3 are from 20 - 500 MPa and 0 to 360 MPa, and for 375 m/5000yr, average limits for σ_1 and σ_3 belong to 60 - 800 MPa and 0 to 600 MPa respectively, which indicates that the difference between maximum principal stress (σ_1) and minimum principal stress (σ_3) is comparatively high if the convergence rate is relatively high and the deformation rate is also strong. The results are observed from the stress field over the Granitic layer, Tethys Himalaya, Higher Himalaya, Lesser Himalaya and Siwalik that the principal stresses are stronger in the deeper part than the shallower one. For models 3(A) and 3(B) hydrostatic condition is observed along the granitic layer beneath the Siwalik for the boundary condition 75 m during 1000 yr but for 375 m during 5000 yr hydrostatic condition belongs to some parts of granitic layer and deeper most part of Higher Himalaya and Lesser Himalaya. For model - 2, hydrostatic condition is observed along the upper part of Higher Himalaya and some parts of Lesser Himalaya for the boundary condition 75 m/1000yr. But for 375 m/5000yr hydrostatic condition is obtained in the deeper part of Higher Himalaya and Lesser Himalaya along the MCT and MBT zones. Hydrostatic condition is obtained along the deeper and upper most part of Higher Himalaya according to the boundary condition 375 m/5000yr and 75 m/1000yr, respectively for the model - 1. It is obvious from the discussion that no deformation is observed along the deeper part of Lesser Himalaya, Higher Himalaya and Granitic layer due to hydrostatic condition. May be, lower parts of these layers belong to a high grade metamorphic rock.

The occurrence of faulting under Mohr circle depends on the values of displacement boundary condition, cohesive strength (c) and friction angle (ϕ). The values of cohesive strength (c) and friction angle (ϕ) are shown in Tables 2-4. When the displacement boundary condition is equal to 75 m/1000yr no failure may occur for all the models but if gradual change of boundary condition i.e. 150 m/2000yr, 225 m/3000yr then a few failure may occur at the shallower level. For the proposed models, displacement boundary condition has been taken as 375 m/5000yr. Depending on this condition some failure occur along the shallower level of all the models and most of the failure occur at the sub Himalaya and the Tethys Himalaya (Fig. 24-27). According to the predetermined great thrusts (MBT, MCT, LHT and STDS), failure occur along two boundaries (Fig. 24-27).

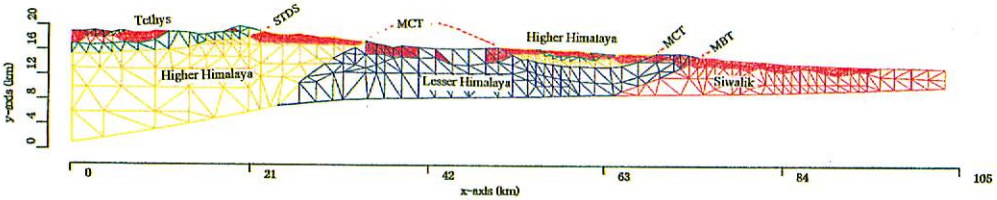

Fig. 24. Failure elements of model - 1. Red blocks indicate failured.

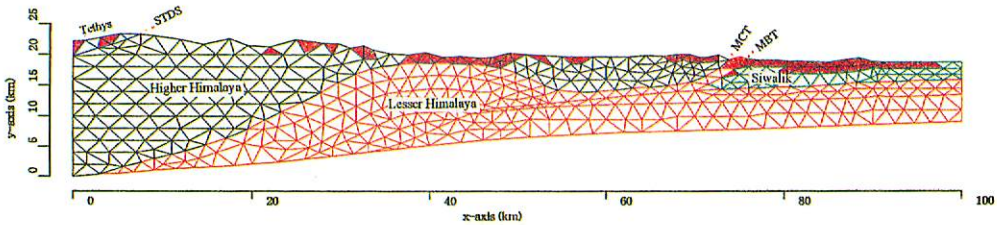

Fig. 25. Failure elements of model - 2. Red blocks indicate failured.

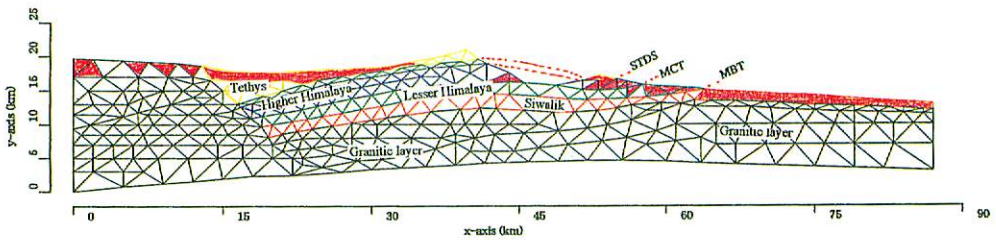

Fig. 26. Failure elements of model - 3(A). Red blocks indicate failured.

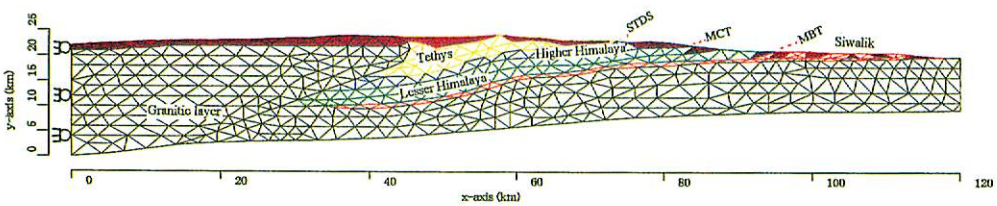

Fig. 27. Failure elements of model - 3(B). Red blocks indicate failured.

By 'tuning' different controlling parameters, we did not succeed in obtaining in a model where failure occurred at the deeper part of Higher Himalaya and Lesser Himalaya, due to hydrostatic condition.

Several published studies of focal mechanism solutions of earthquakes in the Himalaya region give the same general pattern of thrust faulting, with one plane dipping gently beneath the Himalaya (Armbruster et al., 1976; Banghar, 1974; Ben Menahen et al., 1974; Chen & Molnar, 1977; Fitch ,1970; Ichikawa et al., 1972; Molnar et al., 1973; Rastogi et al., 1973; Tandon & Srivastava, 1975).

This study also shows the same pattern of thrust faulting along the shallower part

of all the models. The boundary condition, whatever it might be (75 m during 1000yr or 375 m during 5000 yr), it shows thrust faulting along the shallower region of the Himalaya. Changing of displacement boundary condition changes the direction of principal stresses along the deeper part but the upper part remain unchanged.

Conclusion

(1) Variation of the velocity boundary condition indicates changes of direction of principal stresses along the deeper part while that along the shallower part remain unchanged.

(2) Nature of stress pattern is most likely compressive for all the models but if convergence rate is high then some extension (less than 100 MPa) may happen on the shallower part.

(3) The difference between maximum principal stress (σ_1) and minimum principal stress (σ_3) is comparatively high if the convergence rate is relatively high.

(4) Hydrostatic condition occurs within the deeper part of the Higher Himalaya, Lesser Himalaya and some parts of the Granitic layer (no deformation may occur within the region).

(5) General tendency of the direction of principal stresses (σ_1 and σ_3) are complicate to determine. Along the upper part of the whole region the maximum principal stress is horizontal. Comparatively, in the lower part, the direction of principal stress is vertical (except for the boundary condition 375m).

(6) According to the Mohr - Coulomb criterion, failure is observed along the shallower part of Siwalik, Tethys and Granitic layer, and a very few near the surface of MBT, MCT and STDS.

(7) Inspite of changing the controlling parameters, failure did not occur in the deeper part of Higher Himalaya, Lesser Himalaya and Granitic layer, because of hydrostatic condition.

(8) Previous studies on focal mechanism solutions of earthquakes in the Himalayan region show the existence of thrust faults along its EW stretching with one plane dipping gently north beneath the Himalaya. Simulation provides the same distribution of thrust faults along the upper part of the models as shown by the focal mechanism solutions.

Acknowledgment

Md. Mahmudul Alam would like to express his gratitude to MONBUSHO for financial constraint during the study period. The encouragement and suggestions for him received from honorable teacher Professor Massaki Kimura, Department of Physics and Earth Sciences, University of the Ryukyus, Okinawa, Japan.

References

Arita, K., Hayashi, D., Yoshida, M., 1982. Geology and structure of the Pokhara-Piuthan

area, central Nepal. *Jour. Nepal Geol. Soc.* **2**, 5-29.

Arita, K., Shiraishi, K. Hayashi, D., 1984. Geology of western Nepal and a comparison with Kumaun, India. Jour. FAc. Sci., Hokkaido Univ. Ser. IV. 21(1), 1-20.ture of the Pokhara-Piuthan area, central Nepal. *Jour. Nepal Geol. Soc.* **2**, 5-29

Arita, K., 1983. Origin of the inverted metamorphism of the lower Himalaya, central Nepal. *Tectonophysics*, **95**, 43-60.

Armbraster, J., Seeber, L., Jacob, K.H., 1978. The northwestern termination of the Himalayan mountain front: Active tectonics from microearthquakes. *J. Geophys. Res.* **83**, 269-282.

Banghar, A.R., 1974. Focal mechanisms of earthquakes in China, Mongolia, Russia, Nepal, Pakistan, and Afghanistan. *Earthq. Notes*, **45**, 1-11.

Banghar, M. Isacks, B.L., 1976. Spatial distribution of earthquakes and subduction of the Nazca plate beneath South America. *Geology*, **4**, 686-692.

Bashyal, R.P., 1981. Geology of Dhangarhi-Dandeldhura road section and its regional significance. *JNGS*, **1**, 15-28.

Bordet, P., Colchen, M., Le Fort, P., 1972. Some features of the geology of the Annapurna renge, Nepal Himalaya. *Him. Geol.*, **2**, 537-563.

Brunet, M., 1986. Ductile thrusting in the Himalayas: Shear sense criteria and stretching lineations. *Tectonics*, **5**, 247-265.

Burg, J.P., Chen, G.M., 1984. Tectonics and structural zonation of southern Tibet, China. *Nature*, **311**, 219-223.

Chandra, U., 1981. Focal mechanism solutions and their tectonic implications for the eastern Alpine-Himalayan region. *Geodynamics series*, **3**, 243-271.

Chemenda, A.I., Mattaure, M. Malavieille, J., Bokun, A.,N., 1995. A mechanism for syn-collisional rock exhumation and associated normal faulting: Results from physical modeling. *Earth Planet. Sci. Lett.*, **132**, 225-232.

Chen, W.P., Molnar, P. 1977. Seismic moments of major earthquake and the average rate of slip in central Asia. *J. Geophys. Res.*, **82**, 2945-2969.

Colchen, M., LE Fort, P., Pecher, A., 1986. Geological research in the Nepal's Himalaya: Annapurna-Manaslu-Ganesh Himal, notice of the geological map on 1/200000. *Centre National de la Recherche Scientifique*, Paris.

Dewey, J.F., Bird, J.M., 1970. Mountain belts and the new global tectonics. *J. Geophys. Res.*, **75**, 2625-2647.

England, P., Houseman, G., 1985. Role of lithospheric strength heterogeneities in the tectonics of Tibet and neighbouring regions. *Nature*, **315**, 297-301.

England, P., Houseman, G., 1986. Finite strain calculations of continental deformation, 2, comparison with the India-Asia collision zone. *J. Geophys. Res.*, **91**, 3664-3676.

England, P., Mckenzie, D., 1982. A thin viscous sheet model for continental deformation. *Geophys. J.R.Astr.Soc.*, **70**, 295-321.

England, P., Mckenzie, D., 1983. Correction to a thin viscous sheet model for continental deformation. *Geophys. J.R.Astr.Soc.*, **73**, 523-532.

England, P.C., Thomson, A.B., 1984. Pressure - temperature-time paths of regional metamorphism, part-I: Heat transfer during the evolution of regions of thickened continental crust. *Jour. Petrol.*, **25**, 929-954.

Evans, P., 1964. The tectonic framework of Assam, *J. Geol. Soc. India*, **5**, 80-96.

Fitch, T.J., 1970. Earthquake mechanisms in the Himalaya, Burmese and Andaman regions and continental tectonics in Central Asia. *J. Geophys. Res.*, **75**, 2699-2709.

Fuchs, G., Frank, W., 1970. The geology of west Nepal between the rivers Kali Gandaki and Thulo Bheri. Jahrb. Bundesanst. *Sonderb.* **18**, 1-103.

Fuchs, G., 1980. The Lesser Himalayan geology of west Nepal and its regional importance. In: stratigraphy and correlations of Lesser Himalayan formations, *Hindustan Pub., Delhi*, 163-173.

Ganseer, A., 1964. Geology of the Himalayas. *Interscience*, London 289p.

Ganseer, A., 1966. The Indian Ocean and the Himalayas: a geological interpretation, *Eclog. Geol. Helv.*, **59**, 831-848.

Gill, W.D., 1952. The stratigraphy of the Siwalik Series in the northern Potwar, Punjab, Pakistan. *Q.J. Geol.Soc. London*, **107**(4), 375-394.

Glennie, K.W., Ziegler, M.A., 1964. The Siwalik formation in Nepal. Intern. *Geol. Cong. 22nd Sess. Rep. Pt.*, **15**, 82-95.

Hagen, T., 1969. Report on the geological survey of Nepal, Vol.1. Denkschr. Schweiz. *Naturf. Gesell., Bd.* **86**(1), 1-185.

Hashimoto, S., et al., 1973. Geology of the Nepal Himalayas. **Saikon, Tokyo**, 286p.

Hayashi, D., 1979. Finite element formulation of viscous fluid on a variational principle. *Bull. Coll. Sci. Univ. Ryukyu*, **28**, 119-130.

Hayashi, D., 1980. Variation of field of viscous stress around diapir calculated by the finite element method. *Bull. Coll. Sci. Univ. Ryukyu*, **30**, 11-21.

Hayashi, D., 1980. Simulation of Himalayan orogeny and tectonophysics. *Monthly Earth*, **2**, 787-796.

Hayashi, D., 1987. Numerical simulation of the uplift of the Tibetan Plateau. *Jour. Geol. Soc. Jap.*, **93**, 587-595.

Hayashi, D., Kizaki, K., 1972. Numerical analysis on migmatite dome with special reference to the finite element method. *Jour. Geol. Soc. Jap.*, **78**, 677-686.

Hayashi, D., Kizaki, K., 1979. Numerical experiments of migmatite rise based on continuum dynamics. *Tectonophysics*, **60**, 61-76.

Hayashi, D., Fujii, Y., Yoneshiro, T., Kizaki, K. 1984. Geology of the Karnali-Bheri region, west Nepal. *Jour. Nepal Geol. Soc.*, **2**, 29-40.

Hayashi, D., Talbot, C., 1991. Numerical simulation of a Himalayan profile. *Essays in Geology, Professor Hisao Nakagawa Commemorative Volume*, 53-63.

Hiroshima, M., 1972. Topography of Marsyandi River, *Symposium: Nepal* , 1, 45-50.

Ichikawa, M., Srivastava, H.N., Drakopoulos, J., 1972. Focal mechanism of earthquakes occuring in and around Himalayan and Burmese mountain belt. *Papers in Meteorology and Geophysics (Tokyo)*, **23**, 149-162.

Isacks, B.L., Oliver, J., Sykes, L.R., 1968. Seismology and the new global tectonics. *J. Geophys. Res.*, **73**, 5855-5900.

Itihara, M. Shibasaki, T., Miyamoto, N., 1972. Photogeological survey of the Siwalik Ranges and the Terai Plain, southeastern Nepal. *Jour. Geosci. Osaka City Univ.*, **15**, 77-98.

Ito, H., 1972. Change of topography due to flow of the crust under the condition of isostasy. Jour. *Geol. Soc. Jap.*, **78**, 29-38.

Kamada, K., Yashida, M., Arita, K., 1982. Jurassic ammonites from the Muktinath region. *Jour. Nepal Geol. Soc.*, **2**, 149-154

Kaneko, Y., 1994. Metamorphic P-T path of the Higher Himalayan Sequence in the Annarnapurna region, central Nepal Himalaya. Proceeding of the *Himalaya Symposium*, Tokai University Press.

Kaneko, Y., 1995. Thermal structure in the Annapurna region, central Nepal Himalaya: implication for the inverted metamorphism. *Jour. Mineral. Petrol. Econ. Geol.*, **90**, 143-154.

Kano, T., 1977. Origin of augen gneisses and related mylonitic rocks in the Hida metamorphic

region, central Japan. *Plutonism in relation to volcanism and metamorphism* (7th C.P.P.P. meetings), 206-229.

Le Fort, P., 1975. Himalayas: the collided range. Present knowledge of the continental arc. *Amer. Jour. Sci.*, **275**, 1-44.

Le Pichon, X., 1968. Sea floor spreading and continental drift. J. Geophys. Res. 73, 3661-3698.

McKenzie, D., 1969. Speculations on the consequences and causes of the plate motions. Geophys. *J. Roy. Astr. Soc.*, **18**, 1-32.

Menke, W.H., Jacob, K.H., 1976. Seismicity patterns in Pakistan and northwestern India associated with continental collision. *Bull. Seismo. Soc. Amer.* 76.

Minster, J.B., Jorden, T.H., Molnar, P., Haines, E., 1974. Numerical modeling of instantaneous plate tectonics. *Geophys. J. Roy. Astr. Soc.*, **36**, 541-576.

Molnar, P., Fitch, T.J., Wu, F.T., 1973. Fault plane solutions of shallow earthquakes contemporary tectonics of Asia. *Earth Plan. Sci. Lett.*, **16**, 101-112.

Molnar, P., Fitch, T.J., Wu, F.T., Chen, W.P., Warsi, W.E.K., Tapponnnier, P., 1977. Structure and tectonics of the Himalaya; A brief summary of relevant geophysical observations. Himalaya, *Science de la Terre, Centre National de la Recherche Scientique*, Paris, 269-294.

Molnar, P., Tapponnnier, P., 1975. Cenozoic tectonics of Asia: effect of a continental collision. *Science*, **189**, 419-426.

Pecher, A., 1989. The metamorphism in the central Himalaya. *Jour. Metamorphic. Geol.*, **7**, 31-41.

Powell, P., Conaghan, P.J., 1973. Plate tectonics and the Himalayas. *Earth Plan. Sci. Lett.*, **20**, 1-20.

Rastogi, B.K., 1974. Earthquake mechanisms and plate tectonics in the Himalayan region. *Tectonophysics*, **21**, 47-56.

Sakai, H., 1985. Geology of the Kali Gandaki Supergroup of the Lesser Himalaya in Nepal. *Mem. Fac. Sci., Kyushu Univ., Ser. D. Geol.*, **25**, 337-397.

Searly, M., Windley, B.F., Coward, M.P., Cooper, D.J.W., Rex, A.J., Rex, D., Tingdong, L., Xuchang, X., Jan. M.M.Q., Thakur, V.C. and Kumar, S., 1987. The closing of Tethys and the tectonics of the Himalaya. *Bull. Geol. Soc. Amer.*, **98**, 678-701.

Seeber, L., Armbruster, J.G., Quittmeyer, R.C., 1981. Seismicity and Continental subduction in the Himalayan Arc. *Geodynamics series*, **3**, 215-242.

Sharma.T., Merh, S.S., Vashi, N.M., 1978. The Terraced Conglomerates of Pokhara Vally in central Nepal, *Symposium on Morphology and Evolution of Landforms*, Department of Geology, University of Delhi, 226-240.

Sharma.T., Upreti, B.N., Vashi, N.M., 1980. Kali Gandaki gravel deposits of central West Nepal - their neotectonic significance, *Tectonophysics*, **62**, 127-139.

Stauder, W., 1968. Tensional character of earthquake foci beneath the Aleutian trench with relation to sea-floor spreading. *J. Geophys. Res.*, **73**, 7693-7703.

Stocklin, J., 1980. Geology of Nepal and its regional frame. *Jour. Geol. Soc. London*, **137**, 1-34.

Tandon, A.N., Srivastava, H.N., 1975. Focal mechanisms of some recent Himalayan earthquakes and regional plate tectonics. *Bull. Seismo. Soc. Amer.*, **65**, 963-969.

Tandon, S.K., 1976. Siwalik sedimentation in a part of the Kumaun Himalaya, India. *Sed. Geol.*, **16**, 131-154.

Tandon, S.K., Narayan, D., 1981. Calcrete conglomerate, case-hardened conglomerate and cornstone, a comparative account of pedogenic carbonates from the continental Siwalik

Group, Punjab, India. *Sedimentology*, 28, 353-367.

Tapponnier, P. Molnar, P., 1977. Active faulting and tectonics in China. *J. Geophys. Res.*, 82, 2905-2930.

Uemura, T., 1971. Some problems on tectonic flow of rocks. Jour. Geol. Soc. Jap. 77, 273-278.

Valdiya, K.S., 1980. Geology of Kumaun Lesser Himalaya. *Wadia Institute of Himalayan Geology, Dehra Dun, India*, 291p.

Valdiya, K.S., 1977. Structural set-up of the Kumaun Lesser Himalaya. In: *Himalaya, C.N.R.S., Paris*, 449-462.

Valdiya, K.S., 1980. Outline of the structure of Kumaun Lesser Himalaya. In: Tectonic geology of the Himalaya. *Today and Tomorrow Pub., New Delhi*, 1-14.

Wadia, D.N., 1975. Geology of India, 4th Edition. Tata McGraw-Hill Publishing Co., New Delhi, 508p.

Warsi, R.I., Molnar, P., 1977. Plate tectonics and gravity anomalies in India and the Himalaya. Science de la Terre, Centre National de la Recherche *Scientique*, Paris.

West, R.M., Lukacs, J.R., Munthe, J.Jr., Hussain, S.T., 1978. Vertebrate fauna from Neogene Siwalik Group, Dang Vally, western Nepal. *Jour. Paleont.*, 52, 1015-1022.

Widely, B.F., 1984. The evolving continents, 2nd ed. *John Wiley and Sons, Inc.*, 399p.

Widely, B.F., 1995. The evolving continents, 3rd ed. *John Wiley and Sons, Inc.*, 526p.

Yamanaka, H., Iwata,S., 1982. River terraces along the middle Kali Gandaki and Marsyandi Khola, central Nepal. *Jour. Nepal Geol. Soc.*, 2, 95-111.

Yamanaka, H., Yoshida, M., Arita, K., 1982. Terrace landform and Quaternary deposit around Pokhara vally, central Nepal. *Jour. Nepal Geol. Soc.*, 2, 113-136.

Yashida, M., Arita, K., 1982. On the Siwaliks observed along some routes in central Nepal. *Jour. Nepal Geol. Soc.*, 2, 59-66.